

Fast, Scalable Approximations to Posterior Distributions in Extended Latent Gaussian Models

Alex Stringer*

and

Patrick Brown

Department of Statistical Sciences, University of Toronto

Centre for Global Health Research

and

Jamie Stafford

Department of Statistical Sciences, University of Toronto

Abstract

We define a novel class of additive models called Extended Latent Gaussian Models and develop a fast, scalable approximate Bayesian inference methodology for this class. The new class covers a wide range of interesting models, and the new methodology is better suited to large samples than existing approaches. We discuss convergence theory for our posterior approximations. We then illustrate the computational aspects of our approach through a comparison to existing methods, and demonstrate its application in three challenging examples: the analysis of aggregated spatial point process data, the fitting of a Cox proportional hazards model with partial likelihood and a latent spatial point process, and an astrophysical model for estimating the mass of the Milky Way in the presence of multivariate measurement uncertainties. Computations make use of the publicly available `aghq` package in the R language and code for the examples in the paper is available from <https://github.com/awstringer1/elgm-paper-code>.

Keywords: Additive model; Approximate inference; Bayesian methods; Laplace approximation; Spatial statistics.

*The authors gratefully acknowledge funding from the Natural Sciences and Engineering Research Council of Canada.

1 Introduction

Latent Gaussian Models (LGMs) are a class of additive regression models that are of broad interest in modern practice. However, they are limited to likelihoods with a specific dependence structure between the mean response and the additive predictor. Inspired by the well-known methods of Rue et al. (2009) for approximate Bayesian inference in LGMs, Stringer et al. (2020) develop an approximate Bayesian inference method for a type of additive model with a more complex likelihood than LGMs permit. In Stringer et al. (2020)’s implementation, they found that certain computational strategies employed by Rue et al. (2009) to achieve efficient approximate Bayesian inference in LGMs become computationally burdensome when considering this more complicated model. In order to develop approximate Bayesian inference methods that work for a broader class of models than LGMs, a novel approach is required.

Specifically, Rue et al. (2009) add a small amount of Gaussian noise to the additive predictor in all models fit using their approximations. Adding this noise means that the size of all matrices which must be stored and decomposed during fitting now depends linearly on n , the sample size. Critically, in LGMs the Hessian of the log-likelihood is a diagonal matrix, which improves the feasibility of this strategy. When moving beyond the class of LGMs to models with more complicated dependence structures, however, this is no longer the case, and adding this Gaussian noise forces the storage and decomposition of large *dense* matrices during model fitting, leading to adding computational burden which becomes worse as n increases. It also makes the theoretical aspects of the approach more difficult to study due to the challenge of quantifying the asymptotic behaviour of the Laplace approximation in high dimensions (Shun and McCullagh, 1995). Stringer et al. (2020) include the Gaussian noise for their model and observe an increase in memory requirements of their procedure as n increases because of this. Bilodeau et al. (2021, §7) briefly consider a similar approximation in a related application but without this noise term, demonstrating the feasibility of inference without it.

In this paper we introduce the class of Extended Latent Gaussian Models (ELGMs) and provide an approximate Bayesian inference method for this class which avoids the

computational burden introduced by the noisy additive predictor. In ELGMs we allow a much more general type of dependence between the mean response and the additive predictor than in LGMs, which leads to a much broader class of models but also less sparsity in the matrices required to fit the approximations. Critically, our new method involves computations on matrices of reduced size when compared to the methods of Rue et al. (2009) and Stringer et al. (2020), and this size is not forced by the method to scale with n . This leads to approximations which work for the broader class of ELGMs, and when applied to LGMs exhibit faster run times and scale to large datasets. We compare computation times to Rue et al. (2009) by fitting a large generalized linear mixed model to datasets of increasing size, finding that at large sample sizes the reduced size of the matrices involves leads to our method having faster run times. We also discuss convergence theory for the approximations, noting that while this is a highly nontrivial subject (as discussed in Bilodeau et al. (2021, §7)), removal of the Gaussian noise term makes its study more feasible.

We apply our new methodology to fit three challenging models which are beyond the class of LGMs but belong to the new class of ELGMs. We fit a fully Bayesian analysis of aggregated spatial point process data, a challenge which Li et al. (2012) and others address using data augmentation techniques and MCMC; the existence of software for doing so in this example enables direct comparison of our method with MCMC techniques where we make similar inferences at substantial reduction in computational cost. We fit a Cox proportional hazards model with partial likelihood and spatially-varying hazard; previous analyses of these data employ parametric (Henderson et al., 2002; Lindgren et al., 2011) and semi-parametric (Martino et al., 2011) models for the hazard due to the difficulty of working with both the partial likelihood and the latent spatial process. Finally, we fit the Galactic Mass Estimation model of Eadie et al. (2017) and Eadie and Juric (2019) for estimating the mass of the Milky Way galaxy in the presence of multivariate measurement errors. Implementation makes use of the publicly available `aghq` package in the R language (Stringer, 2021) and code for all examples is made available at <https://github.com/awstringer1/elgm-paper-code>.

The remainder of the paper proceeds as follows. In §2 we define the class of LGMs and briefly describe existing approaches to approximate Bayesian inference for them. In §3 we define the class of ELGMs and the method for approximate Bayesian inference that we use to fit them in the present work, and in §4 we discuss theoretical considerations. In §5 we provide numerical approaches to existing methods and in §6 we analyze our three stated examples. We conclude in §7 with a discussion of the impact of our contributions and avenues of future research.

2 Preliminaries

In what follows, for any $n \in \mathbb{N}$ we let $[n] = \{1, \dots, n\}$. We use the notation \mathbf{v} for any vector $\mathbf{v} = \{v_i : i \in [n]\}$ with components v_i and for any set $S \subseteq [n]$ let $\mathbf{v}_S = \{v_i : i \in S\}$.

2.1 Latent Gaussian Models

Rue et al. (2009) introduce a class of additive regression models, which they call Latent Gaussian Models (LGMs), where a response Y_i has likelihood $\pi(Y_i|\eta_i, \boldsymbol{\theta}_1)$, and the mean of Y_i is related to an additive predictor η_i through a link function. Latent Gaussian Models take the following form:

$$\begin{aligned} Y_i|\eta_i, \boldsymbol{\theta}_1 &\stackrel{ind}{\sim} \pi(Y_i|\eta_i, \boldsymbol{\theta}_1), \\ \mu_i &= \mathbb{E}(Y_i|\eta_i, \boldsymbol{\theta}_1) = g(\eta_i), \\ \eta_i &= \mathbf{x}_i^T \boldsymbol{\beta} + \sum_{q=1}^r u_q(z_{iq}), \end{aligned} \tag{1}$$

where $i \in [n]$ and $g : \mathbb{R} \rightarrow \mathbb{R}$ is an (inverse) link function. A critical assumption of this model is that the Y_i are conditionally independent given η_i , and in §3 we extend this model to much more complex dependence structures for Y_i . Here $\mathbf{x}_i \in \mathbb{R}^p$ are covariates, and $\boldsymbol{\beta} \in \mathbb{R}^p$ are regression coefficients (which may include an intercept) with prior distribution $\boldsymbol{\beta} \sim N(0, \boldsymbol{\Sigma}_\beta)$. In typical applications $\boldsymbol{\Sigma}_\beta$ is taken to be diagonal. The vector $\boldsymbol{\theta}_1 \in \mathbb{R}^{s_1}$, which includes a small number s_1 of additional parameters relating to the distribution of Y_i , is given prior distribution $\pi(\boldsymbol{\theta}_1)$.

Each $u_q(\cdot)$, $q \in [r]$ is an unknown function of covariate $z_{iq} \in \mathbb{R}$, and the generality of this definition means that many models fall under this framework. In an LGM inferences are made for the finite-dimensional parameter vectors $\mathbf{U}_q = \{u(z_{iq}) : i \in [n]\}$, each of which have d_q unique values and are given Gaussian prior distributions:

$$\mathbf{U}_q | \boldsymbol{\theta}_2 \sim \text{N} [0, \boldsymbol{\Sigma}_{\mathbf{U}_q}(\boldsymbol{\theta}_2)] ,$$

independently for each $q \in [r]$. This leads to a parameter vector $\mathbf{U} = \{\mathbf{U}_q : q \in [r]\}$ with dimension $d = \sum_{q=1}^r d_q$ and prior $\mathbf{U} | \boldsymbol{\theta}_2 \sim \text{N} [0, \boldsymbol{\Sigma}_{\mathbf{U}}(\boldsymbol{\theta}_2)]$ where

$$\boldsymbol{\Sigma}_{\mathbf{U}}(\boldsymbol{\theta}_2) = \text{blockdiag} \{ \boldsymbol{\Sigma}_{\mathbf{U}_q}(\boldsymbol{\theta}_2) : q \in [r] \} .$$

The vector $\boldsymbol{\theta}_2 \in \mathbb{R}^{s_2}$ of covariance parameters for \mathbf{U} is given prior distribution $\pi(\boldsymbol{\theta}_2)$. Examples of the relationship between a single $u(\cdot)$ and \mathbf{U} ($r = 1$ and dropping the subscript q for brevity) include:

1. *Random-intercepts* (§5): each observation comes from one of d groups with group intercepts U_1, \dots, U_d . The covariate $z_i \in [d]$ is the index of the group to which observation i belongs, $u(z_i) \equiv U_{z_i}$, and (hence) $u(\cdot)$ takes one of d distinct values.
2. *Continuous variation* (§6.2): $u(\cdot)$ is a (random) continuous function over \mathbb{R}^p , $u(z_i)$ takes distinct values for each distinct z_i , and $d = n$.
3. *Discrete variation* (§6.1): $u(\cdot)$ is modelled as piecewise-constant on a grid (or otherwise) with cells $\mathcal{Q}_l, l \in [d]$ and cell values U_l such that $u(z_i) \equiv U_l$ whenever $z_i \in \mathcal{Q}_l$, and again $u(\cdot)$ takes one of d distinct values.

Concrete examples of the functions $u(\cdot)$ and corresponding parameters \mathbf{U} are given in §5 and §6.

For clarity it is convenient to write the entire model in vector form. Define the *Gaussian variables* $\mathbf{W} = (\mathbf{U}, \boldsymbol{\beta})$ with dimension $m = d + p$. The distribution of $\mathbf{W} | \boldsymbol{\theta}_2$ is then

$$\mathbf{W} | \boldsymbol{\theta}_2 \sim \text{N} (0, \mathbf{Q}_{\boldsymbol{\theta}_2}^{-1}) ,$$

where the precision matrix $\mathbf{Q}_{\boldsymbol{\theta}_2}$ inherits any sparsity from $\boldsymbol{\Sigma}_{\mathbf{U}}^{-1}(\boldsymbol{\theta}_2)$, which in turn is prescribed (or not) by the specific models for the $u_q(\cdot)$. In what follows it becomes convenient

to work with the vector of additive predictors $\boldsymbol{\eta} = \{\eta_i : i \in [n]\}$ which can now be written as $\boldsymbol{\eta} = \mathbf{Z}\mathbf{W}$ where $\mathbf{Z} \in \mathbb{R}^{n \times m}$ is a fixed, known design matrix constructed from \mathbf{x}_i and z_{iq} . Finally, denote the vector of *nonlinear parameters* as $\boldsymbol{\theta} = (\boldsymbol{\theta}_1, \boldsymbol{\theta}_2)$ with dimension $s = s_1 + s_2$ and prior distribution $\pi(\boldsymbol{\theta}) = \pi(\boldsymbol{\theta}_1)\pi(\boldsymbol{\theta}_2)$.

2.2 Posterior approximations

The posterior distribution of the Gaussian variables may be written:

$$\pi(\mathbf{W}|\mathbf{Y}) = \int \pi(\mathbf{W}|\mathbf{Y}, \boldsymbol{\theta})\pi(\boldsymbol{\theta}|\mathbf{Y})d\boldsymbol{\theta}. \quad (2)$$

Inference for \mathbf{W} is based off of (2) including marginal point and interval estimates for its components $W_j, j \in [d]$, although the full joint posterior is useful for calculating certain complicated posterior summaries of interest as well (§6.1, §6.2). The joint posterior distribution of the nonlinear parameters is:

$$\pi(\boldsymbol{\theta}|\mathbf{Y}) = \int \pi(\mathbf{W}, \boldsymbol{\theta}|\mathbf{Y})d\mathbf{W} = \frac{\int \pi(\mathbf{W}, \boldsymbol{\theta}, \mathbf{Y})d\mathbf{W}}{\int \int \pi(\mathbf{W}, \boldsymbol{\theta}, \mathbf{Y})d\mathbf{W}d\boldsymbol{\theta}}, \quad (3)$$

which is primarily used to assess posterior uncertainty in components of $\boldsymbol{\theta}$ and appears in the integrand of (2), although there are also examples where this posterior is of more direct interest (§6.3).

Approximating the posterior (2) is facilitated by a Gaussian approximation for $\pi(\mathbf{W}|\mathbf{Y}, \boldsymbol{\theta})$ for each fixed $\boldsymbol{\theta}$ and a Laplace approximation for $\pi(\boldsymbol{\theta}|\mathbf{Y})$ (Tierney and Kadane, 1986). Combining these with numerical integration yields the following approximation for $\pi(\mathbf{W}|\mathbf{Y})$:

$$\tilde{\pi}(\mathbf{W}|\mathbf{Y}) = \sum_{k=1}^K \tilde{\pi}_g(\mathbf{W}|\mathbf{Y}, \boldsymbol{\theta}^k) \tilde{\pi}_{\text{LA}}(\boldsymbol{\theta}^k|\mathbf{Y}) \omega_k. \quad (4)$$

where $\boldsymbol{\theta}^k$ are points and ω_k are weights corresponding to a quadrature rule, the choice of which has important theoretical and practical consequences. Rue et al. (2009) describe two options for this. More recently Stringer et al. (2020) employ adaptive Gauss–Hermite quadrature, which has recently been shown to both be a practically attractive technique and to satisfy strong convergence properties when used for Bayesian inference (Bilodeau et al., 2021), and has been made available in standalone open-source software (`aghq` package,

Stringer (2021)). Further details of the approximation (4) are provided in §2.3 as well as Algorithm 1 in §3.2.

While Rue et al. (2009) and, more recently, Wood (2020) focus on accurate analytical approximations to the marginal distributions derived from $\tilde{\pi}(\mathbf{W}|\mathbf{Y})$, in the present setting we focus on making inferences using the full joint distribution. Specifically, we use standard methods (Rue, 2001) to draw independent samples from the approximate joint posterior, which allows us to estimate any posterior summary of interest. We note that this ability is a principle practical advantage of classical MCMC techniques, one wish we wish to retain in our approach to approximate Bayesian inference. We demonstrate the utility of this approach in our examples (§6.1 and §6.2) and investigate its empirical accuracy via comparison to MCMC (§6.1).

2.3 Sparsity and the Noisy Additive Predictor

Computation of the desired posterior approximations requires the following quantities:

$$\begin{aligned}\widehat{\mathbf{W}}_{\boldsymbol{\theta}} &= \operatorname{argmax}_{\mathbf{W}} \log \pi(\mathbf{W}, \mathbf{Y}, \boldsymbol{\theta}), \\ \mathbf{H}_{\boldsymbol{\theta}}(\mathbf{W}) &= -\partial_{\mathbf{W}}^2 \log \pi(\mathbf{W}, \mathbf{Y}, \boldsymbol{\theta}) = -\partial_{\mathbf{W}}^2 \{ \log \pi(\mathbf{W}|\boldsymbol{\theta}_2) + \log \pi(\mathbf{Y}|\mathbf{W}, \boldsymbol{\theta}_1) \}, \\ &= \mathbf{Q}_{\boldsymbol{\theta}_2} + \mathbf{C}_{\boldsymbol{\theta}_1}(\mathbf{W}), \\ \mathbf{C}_{\boldsymbol{\theta}_1}(\mathbf{W}) &= -\partial_{\mathbf{W}}^2 \log \pi(\mathbf{Y}|\mathbf{W}, \boldsymbol{\theta}_1) = \mathbf{Z}^T \mathbf{C}_{\boldsymbol{\theta}_1}(\boldsymbol{\eta}) \mathbf{Z}, \\ \boldsymbol{\eta} &= \mathbf{Z}\mathbf{W}; \quad \mathbf{Z} = \frac{\partial \boldsymbol{\eta}}{\partial \mathbf{W}}; \quad \mathbf{C}_{\boldsymbol{\theta}_1}(\boldsymbol{\eta}) = -\partial_{\boldsymbol{\eta}}^2 \log \pi(\mathbf{Y}|\mathbf{W}, \boldsymbol{\theta}_1).\end{aligned}$$

The sparsity structure of $\mathbf{H}_{\boldsymbol{\theta}}(\mathbf{W})$ impacts the computational efficiency of inference as its Cholesky decomposition is required both for computation of the Gaussian and Laplace approximations and for finding the mode $\widehat{\mathbf{W}}_{\boldsymbol{\theta}}$. Knowing the sparsity pattern of $\mathbf{H}_{\boldsymbol{\theta}}(\mathbf{W})$ enables the use of efficient numerical techniques for computing this decomposition (for example, reordering to minimize the number of nonzero values in it). Existing software for approximate Bayesian inference such as that of Rue et al. (2009), Stringer et al. (2020) and Stringer (2021) use such techniques to achieve very fast computations in many examples. This sparsity pattern is in turn determined by that of $\mathbf{Q}_{\boldsymbol{\theta}_2}$ and $\mathbf{C}_{\boldsymbol{\theta}_1}(\mathbf{W})$. The exact structure of the prior precision matrix $\mathbf{Q}_{\boldsymbol{\theta}_2}$ is known a-priori, but may be changed by

addition of $\mathbf{C}_{\theta_1}(\mathbf{W})$, complicating matters.

One computational strategy used by Rue et al. (2009) and Stringer et al. (2020) in relation to this challenge is to make inferences based on the following modified model:

$$\begin{aligned}\boldsymbol{\eta}^* &= \boldsymbol{\eta} + \boldsymbol{\epsilon}, \\ \boldsymbol{\epsilon} &\sim \text{N}(0, \tau^{-1} \mathbf{I}_n), \\ \mathbf{W}^* &= (\boldsymbol{\eta}^*, \mathbf{W}) \sim \text{N}(0, \mathbf{Q}_{\theta_2}^{*-1}),\end{aligned}\tag{5}$$

where τ is a large, fixed constant. Under the modified model, the matrices required for computations are:

$$\mathbf{H}_{\theta}^*(\mathbf{W}) = -\partial_{\mathbf{W}^*}^2 \log \pi(\mathbf{W}^* | \mathbf{Y}, \boldsymbol{\theta}) = \mathbf{Q}_{\theta_2}^* + \mathbf{C}_{\theta_1}^*(\mathbf{W}),$$

where now:

$$\mathbf{Q}_{\theta_2}^* = \tau \begin{pmatrix} \mathbf{I}_n & -\mathbf{Z} \\ -\mathbf{Z}^T & \tau^{-1} \mathbf{Q}_{\theta_2} + \mathbf{Z}^T \mathbf{Z} \end{pmatrix}, \quad \mathbf{C}_{\theta_1}^*(\mathbf{W}) = \begin{pmatrix} \mathbf{C}_{\theta_1}(\boldsymbol{\eta}) & 0 \\ 0 & 0 \end{pmatrix},$$

where we recall that $\boldsymbol{\eta} = \mathbf{Z}\mathbf{W}$. Owing to the defining constraint that Y_i are conditionally independent given a single η_i , the matrix $\mathbf{C}_{\theta_1}(\boldsymbol{\eta})$ is diagonal in LGMs. Hence the sparsity pattern of $\mathbf{H}_{\theta}^*(\mathbf{W})$ is exactly that of $\mathbf{Q}_{\theta_2}^*$ in LGMs which employ the modification (5), and prior knowledge of this may be exploited to make these computations more efficient.

When moving to the class of ELGMs, however, the $n \times n$ matrix $\mathbf{C}_{\theta_1}(\boldsymbol{\eta})$ is no longer diagonal and in fact may be dense. The addition of the noise term forces its storage and decomposition during fitting, and this has several implications:

1. It becomes challenging to move beyond LGMs because of the need to store and decompose large, potentially dense matrices,
2. It becomes challenging to fit LGMs to large datasets, because the size of the sparse matrices involved scales linearly with n for every such model fit,
3. It becomes challenging to study the theoretical properties of the approximations, because convergence results pertaining to the marginal Laplace approximation (Tierney and Kadane, 1986) do not apply in this context (Shun and McCullagh, 1995).

Stringer et al. (2020) implement one example of an ELGM in which the use of the modified model (5) is observed to increase the memory requirements of the procedure because of this. Bilodeau et al. (2021) implement a more complicated ELGM but without the noise term, and their computations appear to be more memory-efficient although they do not discuss whether this is the case.

We now define the class of ELGMs and describe our approach to inference for them which avoids these challenges.

3 Extended Latent Gaussian Models

3.1 Definition of ELGMs

In ELGMs the vector of additive predictors is redefined as $\boldsymbol{\eta} = \{\eta_j, j \in [q_n]\}$ to have dimension $q_n \in \mathbb{N}$ depending on, but not necessarily equal to, n . The mean response μ_i , $i \in [n]$ is related to $\boldsymbol{\eta}$ through a many-to-one function $h : \mathbb{R}^{q_n} \rightarrow \mathbb{R}$ in the following manner. Define $\mathcal{J}_i \subseteq [q_n]$ to be the set of indices of $\boldsymbol{\eta}$ upon which μ_i actually depends, which is determined by the likelihood. We then have

$$\mu_i = h(\boldsymbol{\eta}_{\mathcal{J}_i}),$$

where we recall that $\boldsymbol{\eta}_{\mathcal{J}_i} = \{\eta_j : j \in \mathcal{J}_i\}$. By definition we have $\bigcup_{i=1}^n \mathcal{J}_i = [q_n]$ and $1 \leq |\mathcal{J}_i| \leq q_n$ for each $i \in [n]$. Otherwise, the sets \mathcal{J}_i are unrestricted, where in contrast LGMs are defined by the restriction that $\mathcal{J}_i = \{i\}$, $i \in [n]$, and (hence) $q_n = n$. Explicit examples of the sets \mathcal{J}_i are given in §6.

Extended Latent Gaussian Models take the following form:

$$\begin{aligned} Y_i | \boldsymbol{\eta}_{\mathcal{J}_i}, \boldsymbol{\theta}_1 &\stackrel{ind}{\sim} \pi(Y_i | \boldsymbol{\eta}_{\mathcal{J}_i}, \boldsymbol{\theta}_1), i \in [n], \\ \mu_i &= \mathbb{E}(Y_i | \boldsymbol{\eta}_{\mathcal{J}_i}, \boldsymbol{\theta}_1) = h(\boldsymbol{\eta}_{\mathcal{J}_i}), \\ \eta_j &= \mathbf{x}_j^T \boldsymbol{\beta} + \sum_{q=1}^r u_q(z_{jq}), j \in [q_n], \end{aligned}$$

which may be contrasted with the LGM described in §2.1.

The potentially complex dependence between μ_i and $\boldsymbol{\eta}$ introduces computational burden. Specifically, the sparsity pattern of $\mathbf{C}_{\boldsymbol{\theta}_1}(\boldsymbol{\eta})$ is determined by the overlap of the index sets: for any $k, l \in [q_n]$,

$$\exists i \in [n] : k, l \in \mathcal{J}_i \implies \mathbf{C}_{\boldsymbol{\theta}_1}(\boldsymbol{\eta})_{kl} \neq 0.$$

Because of this relationship, the q_n -dimensional $\mathbf{C}_{\boldsymbol{\theta}_1}(\boldsymbol{\eta})$ matrix becomes denser as the model becomes more complex, as specifically measured by the complexity of the index sets \mathcal{J}_i . This in turn affects the computations required for approximate Bayesian inference in ELGMs.

3.2 Computational Considerations

Algorithm 1 shows the full approximation procedure for ELGMs. We highlight some important points here. First, we do not employ the modification (5), and hence the sparsity structure of the Hessian $\mathbf{H}_{\boldsymbol{\theta}}(\mathbf{W})$ is determined both by that of $\mathbf{Q}_{\boldsymbol{\theta}_2}$ and

$$\mathbf{C}_{\boldsymbol{\theta}}(\mathbf{W}) = \mathbf{Z}^T \mathbf{C}_{\boldsymbol{\theta}_1}(\boldsymbol{\eta}) \mathbf{Z},$$

which is (now) of dimension $m \times m$ where $m = \dim(\mathbf{W})$. Note that even in an LGM with diagonal $\mathbf{C}_{\boldsymbol{\theta}_1}(\boldsymbol{\eta})$, $\mathbf{C}_{\boldsymbol{\theta}}(\mathbf{W})$ may not be diagonal when the modification (5) is not made, although it still will often be sparse. The effect of removing $\boldsymbol{\epsilon}$ is therefore to reduce the sparsity, but also reduce the size of these large matrices involved in the calculations. This has the following implications:

1. It becomes feasible to fit ELGMs because the dimension of the large, potentially dense matrices involved in fitting is reduced by n compared to if the modification (5) if employed,
2. It becomes more efficient to fit LGMs to larger datasets because the size of the large, sparse matrices involved in calculations does not scale with n in general,
3. The theoretical properties of the approximation error are more feasible to study (§4) because the convergence of the marginal Laplace approximation is established (Tierney and Kadane, 1986).

We still exploit sparsity when available on a problem-specific basis, using the efficient routines in the `Matrix` package for R (Bates and Maechler, 2019). Further, the reduced *size* of matrices involved is expected to improve computational efficiency of our approximations at larger sample sizes where this difference is more pronounced. We investigate these notions empirically in §5 with a comparison to the software of Rue et al. (2009) for a Bernoulli generalized linear mixed model.

The Laplace approximation $\tilde{\pi}_{\text{LA}}(\boldsymbol{\theta}|\mathbf{Y})$ is obtained by first computing an unnormalized Laplace approximation $\tilde{\pi}_{\text{LA}}(\boldsymbol{\theta}, \mathbf{Y}) \approx \int \pi(\mathbf{W}, \boldsymbol{\theta}, \mathbf{Y}) d\mathbf{W}$ (see Algorithm 1 as well as Tierney and Kadane 1986) and then renormalizing using quadrature. The choice of adaptive Gauss-Hermite quadrature (AGHQ; Naylor and Smith 1982) as the quadrature rule in our method is deliberate and important: it leads to efficient computations due to its high accuracy in general when using a small number of quadrature points (Bilodeau et al., 2021), is made available in standalone software (Stringer, 2021), and may have theoretical benefits in the present context, although further study of it is required to establish this (§4).

Like any other adaptive quadrature rule, implementing AGHQ for this problem requires optimization and two numerical derivatives of $\tilde{\pi}_{\text{LA}}(\boldsymbol{\theta}, \mathbf{Y})$, which is complicated by the fact that each evaluation of this approximation requires further optimization of $\pi(\mathbf{W}, \boldsymbol{\theta}, \mathbf{Y})$ with respect to \mathbf{W} . To compute this mode $\widehat{\mathbf{W}}_{\boldsymbol{\theta}}$ as defined in Algorithm 1 we utilize trust region optimization, with implementations that use sparse (Braun, 2014) or dense (Geyer, 2020) matrix algebra as appropriate in each given application. We find trust region methods to be stable and fast for this problem, and in practice very few iterations seem required to reach convergence. This in turn makes the optimization and renormalization required to compute $\tilde{\pi}_{\text{LA}}(\boldsymbol{\theta}|\mathbf{Y})$ feasible.

4 Theoretical Considerations

It is of interest to consider the convergence of the approximation error in $\tilde{\pi}(\mathbf{W}|\mathbf{Y})$. Specifically, we wish to assert that credible sets computed using this approximation have coverage probabilities which approach their nominal levels as $n \rightarrow \infty$, and characterize for which ELGMs this convergence holds. As noted by Bilodeau et al. (2021, §7), this is a highly

Algorithm 1 Fitting Extended Latent Gaussian Models

Input:

$$\pi(\mathbf{W}, \boldsymbol{\theta}, \mathbf{Y}) = \pi(\mathbf{Y}|\mathbf{W}, \boldsymbol{\theta})\pi(\mathbf{W}|\boldsymbol{\theta})\pi(\boldsymbol{\theta})$$

Define:

$$\widehat{\mathbf{W}}_{\boldsymbol{\theta}} = \operatorname{argmax}_{\mathbf{W}} \pi(\mathbf{W}, \boldsymbol{\theta}, \mathbf{Y}), \mathbf{H}_{\boldsymbol{\theta}}(\mathbf{W}) = -\partial_{\mathbf{W}}^2 \log \pi(\mathbf{W}, \boldsymbol{\theta}, \mathbf{Y}),$$

$$\tilde{\pi}_{\text{LA}}(\boldsymbol{\theta}, \mathbf{Y}) \propto \left| \mathbf{H}_{\boldsymbol{\theta}}(\widehat{\mathbf{W}}_{\boldsymbol{\theta}}) \right|^{-1/2} \pi(\widehat{\mathbf{W}}_{\boldsymbol{\theta}}, \boldsymbol{\theta}, \mathbf{Y}),$$

$$\widehat{\boldsymbol{\theta}} = \operatorname{argmax}_{\boldsymbol{\theta}} \tilde{\pi}_{\text{LA}}(\boldsymbol{\theta}, \mathbf{Y}), \mathbf{H}(\boldsymbol{\theta}) = -\partial_{\boldsymbol{\theta}}^2 \log \tilde{\pi}_{\text{LA}}(\boldsymbol{\theta}, \mathbf{Y}), \mathbf{H}(\boldsymbol{\theta})^{-1} = \mathbf{L}\mathbf{L}^T \text{ (Cholesky)},$$

$K = K_1^s$: number of quadrature points; $\{\mathbf{x}_k, \omega_k^*\}_{k=1}^K$: points and weights from a standard K_1 -point GHQ quadrature rule in s dimensions (Bilodeau et al., 2021, §2.3),

$\boldsymbol{\theta}^k = \mathbf{L}\mathbf{x}_k + \widehat{\boldsymbol{\theta}}, \omega_k = |\mathbf{L}| \omega_k^*, k \in [K]$: AGHQ points and weights (Bilodeau et al., 2021, §2.4).

Do:

1. Find $\widehat{\boldsymbol{\theta}}$ using a quasi-Newton algorithm with gradients estimated using finite differences, and compute $\mathbf{H}(\widehat{\boldsymbol{\theta}})$ using finite differences,
2. Compute the renormalized marginal Laplace approximation:

$$\tilde{\pi}_{\text{LA}}(\boldsymbol{\theta}|\mathbf{Y}) = \frac{\tilde{\pi}_{\text{LA}}(\boldsymbol{\theta}, \mathbf{Y})}{\sum_{k=1}^K \tilde{\pi}_{\text{LA}}(\boldsymbol{\theta}^k, \mathbf{Y}) \omega_k},$$

3. Compute posterior of summaries from $\tilde{\pi}_{\text{LA}}(\boldsymbol{\theta}|\mathbf{Y})$ using analytical methods (Bilodeau et al. (2021), Appendix E),
4. Compute posterior summaries from $\tilde{\pi}(\mathbf{W}|\mathbf{Y})$ by drawing i.i.d. samples:

Input: $B \in \mathbb{N}$, number of samples to draw; $\lambda_k = \tilde{\pi}_{\text{LA}}(\boldsymbol{\theta}^k|\mathbf{Y})\omega_k, k \in [K]$.

For: $b = 1, \dots, B$:

- a. Draw $j \sim \text{Multinomial}(\lambda_1, \dots, \lambda_K)$,
- b. Draw $\mathbf{W}_b \sim \text{N} \left[\widehat{\mathbf{W}}_{\boldsymbol{\theta}^j}, \mathbf{H}_{\boldsymbol{\theta}^j}^{-1}(\widehat{\mathbf{W}}_{\boldsymbol{\theta}^j}) \right]$ (Rue, 2001),

Output: i.i.d. sample $\mathbf{W}_1, \dots, \mathbf{W}_B$ from $\tilde{\pi}(\mathbf{W}|\mathbf{Y})$.

Given $\pi(\mathbf{W}, \boldsymbol{\theta}, \mathbf{Y})$ and its log-derivatives, steps 1. and 2. may be done using the `aghq::marginal_laplace` function, step 3. by using the `summary` method on the resulting object, and step 4. using `aghq::sample_marginal`. See Stringer (2021).

nontrivial question for a variety of reasons. The aim of this section is to provide a detailed and balanced discussion of these challenges in order to understand how existing results may be applied, and which parts are unaddressed in the literature and hence motivate future work.

To this end, in §4.1 we formally state the type of convergence we would like to hold for the ELGM posterior approximation. In Appendix A we decompose the error in the approximation into three parts. For the error introduced by the Gaussian and Laplace approximations, results exist in the literature, and we prove two lemmas which show that these errors converge in probability to zero. For the error introduced by the numerical integration, we observe that existing results (Bilodeau et al., 2021) do not apply in this setting, and we give a heuristic argument for convergence of this term, leaving rigorous establishment for future work.

In §4.2 we briefly discuss the difficulty in developing general convergence theory for ELGMs with specific reference to our examples in §6. Note that discussions of a similar nature appear in Bilodeau et al. (2021, §7) and Rue et al. (2009, §4.1).

4.1 Convergence of ELGM approximate posteriors

Consider the total variation error in the approximation:

$$\|\pi(\mathbf{W}|\mathbf{Y}) - \tilde{\pi}(\mathbf{W}|\mathbf{Y})\|_{\text{TV}} = \sup_{\mathcal{K} \in \mathcal{B}(\mathbb{R}^m)} \left| \int_{\mathcal{K}} \pi(\mathbf{W}|\mathbf{Y}) - \tilde{\pi}(\mathbf{W}|\mathbf{Y}) d\mathbf{W} \right|$$

where $\mathcal{B}(\mathbb{R}^m)$ are the Borel sets in \mathbb{R}^m . A desirable property of the approximation would be $\|\pi(\mathbf{W}|\mathbf{Y}) - \tilde{\pi}(\mathbf{W}|\mathbf{Y})\|_{\text{TV}} \xrightarrow{p} 0$ under reasonable conditions, where the convergence in probability is with respect to the true data-generating process. This would guarantee that approximate credible sets have coverage probabilities which converge to their nominal levels, and that this convergence occurs with high probability over the observed data. In Appendix A we investigate this and highlight several important yet subtle properties of the approximations and the manner in which they interact. We prove two lemmas which handle the contributions to the error of the Gaussian and Laplace approximations using existing results. Particularly challenging, however, is the use of the same quadrature rule to both

normalize $\tilde{\pi}_{\text{La}}(\boldsymbol{\theta}, \mathbf{Y})$ and approximate the integral $\int \tilde{\pi}_{\text{g}}(\mathbf{W}|\mathbf{Y}, \boldsymbol{\theta})\tilde{\pi}_{\text{La}}(\boldsymbol{\theta}|\mathbf{Y})d\boldsymbol{\theta}$. Convergence of the AGHQ approximation depends on expanding the integrand around its mode, and this is not the case for this second integral. It is not a simple matter of applying a new AGHQ rule to this integral at slightly increased computational cost, because a correct centering depends on \mathbf{W} and $\boldsymbol{\theta}$ in a complicated manner and it is not clear how to achieve this in practice. We provide a heuristic argument in Appendix A for the convergence of the quadrature error, leaving its rigorous establishment for future work. We note that these challenges are not unique to AGHQ and are presumably present when applying any adaptive quadrature rule in this context, including the two options given by Rue et al. (2009). However, we argue that in addition to its practical convenience, using AGHQ is desirable from a theoretical perspective since theory pertaining to its use in such complex applications of approximate Bayesian inference is an active area of current research.

Finally, observe that the Laplace approximation is being applied in the manner originally described by Tierney and Kadane (1986), and we apply their result directly. However, in models employing the modification (5), this result does not hold (Shun and McCullagh, 1995), further complicating study of the asymptotic properties of approximate Bayesian inference in that setting.

4.2 Limitations and practical considerations

Aside from the unresolved issues regarding the nonstandard application of AGHQ, any discussion of convergence is further complicated by two factors which apply in most applications of ELGMs in practice, including all of the examples in this paper:

1. If the exact function values $u_q(z_{jq})$ are taken to be the parameters of interest, then \mathbf{W} usually has dimension which scales linearly with n , and
2. If a piecewise constant approximation is instead used for $u_q(z_{jq})$, then the model is *misspecified* in the sense that the model used for inference differs from the model that is assumed to have generated the data.

Complication 1 occurs in Examples 5, 6.2 and 6.3, and invalidates the asymptotic properties

of the Laplace approximation. Shun and McCullagh (1995) study this asymptotic regime and conclude that results have to be proven on a problem-specific basis. Some results do exist, for example Baghishania and Mohammadzadeh (2012) prove the related fact that asymptotic normality holds for the joint posterior $\pi(\mathbf{W}, \boldsymbol{\theta} | \mathbf{Y})$ in certain generalized linear mixed models and include a spatial data example in their analysis. We note again, however, that Complication 1 applies in *every* model which employs the modification (5), which makes the asymptotics of approximations of this type more difficult to study even for simple models in that setting.

Complication 2 occurs in Example 6.1, and makes convergence in probability more difficult to establish. There has been a lot of work on the convergence of specific piecewise approximations to $u_q(z_{jq})$ (see for example Lindgren et al. (2011); Simpson et al. (2016)), but this is naturally a problem-specific consideration, and to our knowledge general results which combine the model error with the error in the posterior approximation have not been established.

5 Computational Comparisons

In this section we compare our procedure (Algorithm 1) to the **R-INLA** implementation of the method of Rue et al. (2009) for a model which both can fit. We find that our procedure runs faster at larger sample sizes, presumably owing to the reduced sizes of matrices involving in fitting.

The **R-INLA** software has many settings that the user can choose to tune the computational details to their specific problems. We use the testing version of **R-INLA** accessed on 2021/02/01 with the **PARDISO** sparse matrix library. Computations were done on a private virtual server with 180 Gb of memory and 16 cores. **R-INLA** and **PARDISO** were run multi-threaded using the `num.threads` and `num.blas.threads` options. The simulations were run with 4, 8, and 16 threads, and the fastest times were observed using 8 threads and these are what we report. We also report the run times of **R-INLA** single-threaded as these were found to be shorter than multi-threaded for large samples. We set `strategy='gaussian'` in **R-INLA** for the fairest comparison of computation time between the two approaches.

We perform our comparisons by fitting a Bernoulli Generalized Linear Mixed Model to a large dataset. A full census of every person who was discharged from a drug or alcohol treatment facility in the United States between 2006 – 2011 and was listed as having used opioids was obtained from the Inter-University Consortium for Political and Social Research through the University of Michigan. The dataset contains person-level records of the year of admission, reason for discharge (including successful completion of the program), and gender, race, and living arrangement (homeless, independent or dependent), for each such person. There are $n = 7,283,575$ records after filtering out missing data. We quantify the association between the probability of a subject successfully completing their program and their gender, race, and living arrangements, using discrete nested random effects to account for correlation between outcomes from subjects living in the same state and the same town.

Denote by Y_i the observed indicator of whether the i^{th} subject completed their treatment, $i = 1 \dots n$, and the vector of covariates for each subject by \mathbf{x}_i . Denote by S_i the state and by T_i the town in which the i^{th} subject lives. There are $d_1 = 47$ states and $d_2 = 262$ towns with reported data. We consider the following model:

$$\begin{aligned} Y_i | \eta_i &\overset{iid}{\sim} \text{Bernoulli}(p_i), i \in [n], \\ \log \left(\frac{p_i}{1 - p_i} \right) &= \eta_i = \mathbf{x}_i^T \boldsymbol{\beta} + u_1(S_i) + u_2(T_i), \\ U_{1,j} | \sigma_1 &\overset{iid}{\sim} N(0, \sigma_1^2), \\ U_{2,j} | \sigma_2 &\overset{iid}{\sim} N(0, \sigma_2^2). \end{aligned} \tag{6}$$

where $\mathbf{U}_1 = \{U_{1j} : j \in [d_1]\}$ and $\mathbf{U}_2 = \{U_{2j} : j \in [d_2]\}$ are the vectors containing the unique values of the state $u_1(S_i)$ and town $u_2(T_i)$ random intercepts, such that for each $i \in [n]$ there is exactly one $j \in [d_1]$ such that $u_1(S_i) = U_{1j}$ and similarly for $u_2(\cdot)$ (§2.1). The regression coefficients all correspond to categorical predictors, with a total of $p = 7 + 1$ non-reference levels and an intercept. The index sets are $\mathcal{J}_i = \{i\}, i \in [n]$ and hence this model is a LGM, compatible with the methodology of Rue et al. (2009). The precision matrix $\mathbf{Q}_{\boldsymbol{\theta}_2}$ and log-likelihood Hessian $\mathbf{C}(\boldsymbol{\eta})$ are both diagonal in this example. The full parameter vector is $\mathbf{W} = (\mathbf{U}, \boldsymbol{\beta})$ where $\mathbf{U} = (\mathbf{U}_1, \mathbf{U}_2) \in \mathbb{R}^d$, and $\dim(\mathbf{W}) = d_1 + d_2 + p = 47 + 262 + 8 = 317$. In contrast, when employing the modification (5) as is done by R-INLA,

$\dim(\mathbf{W}^*) = 317 + n = 7,283,892$ for the full dataset, resulting in much larger matrices to be stored and decomposed during fitting.

We fit this model using our procedure and **R-INLA** to subsets of the data of increasing size. Table 1 shows the results. At large samples, **R-INLA** is much faster when run single-threaded, however our procedure is much faster than either configuration of **R-INLA** due to the reduced size of matrices which must be stored and manipulated. Also shown in Table 1 is the L_2 norm between the posterior means of \mathbf{W} reported by our procedure and **R-INLA** (multi-threaded) scaled by $\dim(\mathbf{W})$, to ensure that the two procedures are giving similar answers despite their differences in computation times.

6 Examples of Extended Latent Gaussian Models

In this section we demonstrate the breadth of the ELGM class and practical utility of our approximate inference method for it through three challenging examples. We fit a point process model to spatially-aggregated data (Li et al., 2012; Nandi et al., 2020) and compare the accuracy of our approach to MCMC. We fit a Cox Proportional Hazards model with partial likelihood for mapping spatial variation in Leukaemia survival times, which is an example of a model in which the Hessian of the log-likelihood is fully dense and hence the most computationally-intensive type of ELGM. We then fit the Galactic Mass Estimator model of Eadie et al. (2017) and Eadie and Juric (2019) for estimating the mass of the Milky Way galaxy in the presence of multivariate measurement uncertainties, a challenging model. All three examples are beyond the class of LGMs but belong to the class of ELGMs. The computations make use of the **aghq** package (Stringer, 2021) in the **R** language, code for all examples is available from <https://github.com/awstringer1/elgm-paper-code>.

6.1 Spatially Aggregated Point Process Data

A spatial point process is a stochastic process which generates random points within a fixed study area. Often, for reasons of privacy or lack of available resources, the exact point locations are not recorded and are instead aggregated to counts within predefined regions

within this area. In such cases, covariate information may be available at a different spatial resolution than the response, complicating inference. Spatial *downscaling* or *disaggregation* is a challenging task where an aggregated response is combined with fine-scale covariate information to infer spatial variation in a phenomenon of interest at a higher resolution than the observed counts. This task has been approached using frequentist methods (Lee et al., 2017; Brown and Stafford, 2021) and Bayesian inference using specialized MCMC algorithms (Li et al., 2012; Diggle et al., 2013).

More recently, Nandi et al. (2020) develop software for approximate Bayesian inference in these models where a single Laplace approximation is used for the joint posterior of all model parameters, making use of the **TMB** package (Kristensen et al., 2016). They describe an example of inferring Malaria incidence in Madagascar using aggregated case counts and fine-scale environmental covariates. We fit this example here within the ELGM framework, obtaining more accurate approximations to the posteriors when compared to a long MCMC run.

Denote the study region of Madagascar by $\mathcal{M} \subset \mathbb{R}^2$ and define an inhomogenous Poisson point process X_s over \mathcal{M} with rate function $\lambda(\cdot)$: $X_s \sim \text{IPP}[\lambda(\cdot); \mathcal{M}]$. We observe case counts $Y_i = \|s : X_s \in S_i\|$ for predefined regions $S_i \subset \mathcal{M}$ with $\cup_{i=1}^n S_i = \mathcal{M}$ and $S_i \cap S_j = \emptyset$ for $i \neq j \in [n]$. For any point location $\mathbf{s} \in \mathcal{M}$ define spatially-varying covariates $\mathbf{x}(\mathbf{s}) : \mathbb{R}^2 \rightarrow \mathbb{R}^p$ (corresponding to elevation, vegetation index and land surface temperature, with $p = 4$ including the intercept) and known population offset function $P(\mathbf{s}) : \mathbb{R}^2 \rightarrow \mathbb{R}$ such that the population in any fixed area $S \subseteq \mathcal{M}$ is $\int_S P(\mathbf{s}) d\mathbf{s}$. We wish to infer incidence risk $\lambda(\cdot)$ using the spatially-aggregated log-Gaussian Cox process:

$$\begin{aligned} Y_i | \lambda(\cdot), v_i &\stackrel{\text{ind}}{\sim} \text{Poisson} \left[\exp(v_i) \int_{S_i} P(\mathbf{s}) \lambda(\mathbf{s}) d\mathbf{s} \right], \\ \log \lambda(\mathbf{s}) &= \beta_0 + \mathbf{x}(\mathbf{s})^T \boldsymbol{\beta} + u(\mathbf{s}), \\ u(\mathbf{s}) &\sim \mathcal{GP} [0, M_\nu(\cdot; \sigma, \rho)], \\ v_i &\stackrel{\text{iid}}{\sim} \text{N}(0, \tau^{-1}), \\ \text{Cov}[u(\mathbf{s} + \mathbf{h}), u(\mathbf{s})] &= M_\nu(\|\mathbf{h}\|; \sigma, \rho), \mathbf{s} \in \mathcal{M}, \mathbf{h} \in \mathbb{R}^2. \end{aligned}$$

Here $M_\nu(\cdot; \sigma, \rho)$ is a Matern covariance function with fixed shape parameter $\nu = 1$ in the

parametrization of Brown (2015). The polygon-level effects v_i are included to account for overdispersion in the polygon counts.

The risk surface $\lambda(\mathbf{s})$ must be discretely inferred, and this requires approximations to the continuously-defined covariates $\mathbf{x}(\mathbf{s})$ and spatial process $u(\mathbf{s})$. For the spatial process we use a basis-function representation (Lindgren et al., 2011):

$$u(\mathbf{s}) \approx \sum_{j=1}^d \psi_j(\mathbf{s}) U_j, \quad (7)$$

where $\psi_j(\cdot)$ are fixed, known piecewise-linear functions and the unknown parameter is $\mathbf{U} = \{U_j : j \in [d]\}$. This approximation is constructed on a *mesh* with triangular cells $\mathcal{M}_j, j \in [d]$ such that $\mathcal{M} \subseteq \cup_{j=1}^d \mathcal{M}_j$ and $\mathcal{M}_j \cap \mathcal{M}_k = \emptyset, j \neq k \in [d]$ (Lindgren and Rue, 2015). See Lindgren et al. (2011) and Lindgren and Rue (2015) for further details.

The covariates are observed on a fine grid with cells $\mathcal{Q}_t, t \in [T]$ such that $\cup_{t=1}^T \mathcal{Q}_t = \mathcal{M}$ and $\mathcal{Q}_t \cap \mathcal{Q}_l = \emptyset$ for $t \neq l \in [T]$. The population counts in each grid cell $P_{it} \equiv \int_{S_i \cap \mathcal{Q}_t} P(\mathbf{s}) d\mathbf{s}$ are available (Figure 1c). Further approximate $x(\mathbf{s}) \approx \mathbf{x}(\mathcal{Q}_t)$ for $\mathbf{s} \in \mathcal{Q}_t$, where $\mathbf{x}(\mathcal{Q}_t)$ is shorthand for taking \mathbf{s} to be the centre of the cell \mathcal{Q}_t . Inferences for $\lambda(\cdot)$ are made on the grid \mathcal{Q}_t by defining $\lambda(\mathbf{s}) \approx \lambda(\mathcal{Q}_t)$ for each $\mathbf{s} \in \mathcal{Q}_t$. Finally, define $\boldsymbol{\lambda} = \{\lambda(\mathcal{Q}_t) : t \in [T]\}$. Figure 1 shows the observed data at the polygon level and on the grid, as appropriate. The discrete model is then:

$$\begin{aligned} Y_i | \boldsymbol{\lambda}_{\mathcal{J}_i}, v_i &\stackrel{iid}{\sim} \text{Poisson} \left(\exp(v_i) \sum_{t \in \mathcal{J}_i} P_{it} \lambda(\mathcal{Q}_t) \right), \\ \mathcal{J}_i &= \{t \in [T] : S_i \cap \mathcal{Q}_t \neq \emptyset\}, \\ \eta_t &= \log \lambda(\mathcal{Q}_t) = \beta_0 + \mathbf{x}(\mathcal{Q}_t)^T \boldsymbol{\beta} + u(\mathcal{Q}_t), \\ u(\mathcal{Q}_t) &= \sum_{j=1}^d \psi_j(\mathcal{Q}_t) U_j, \\ \mathbf{U} | \boldsymbol{\theta}_2 &\sim \text{Normal} [0, \boldsymbol{\Sigma}^{-1}(\boldsymbol{\theta}_2)], \\ v_i &\stackrel{iid}{\sim} \text{N}(0, \tau^{-1}), \end{aligned}$$

where $\boldsymbol{\Sigma}^{-1}(\boldsymbol{\theta}_2)$ is the sparse approximation to the precision matrix of the weights \mathbf{U} on the mesh (Lindgren et al., 2011). Following Nandi et al. (2020) the nonlinear parameters

$\theta = (\log \tau, \log \sigma, \log \rho)$ are assigned priors such that $\tau^{-1/2}, \sigma$ and ρ^{-1} follow independent Exponential distributions chosen to satisfy $\mathbb{P}(\tau > 0.1) = \mathbb{P}(\sigma > 0.1) = \mathbb{P}(\rho < 3) = 0.01$ (which are Penalized Complexity priors of Simpson et al. 2017 and Fuglstad et al. 2019), as well as $\beta_0 \sim N(0, 2^2)$ and $\beta_j \sim N(0, 0.4^2), j \in [p]$ independently.

We fit this model using our ELGM approach (Algorithm 1) with $K = 7$ quadrature points, adapting the excellent software of Nandi et al. (2020) for use with the `aghq` package (Stringer, 2021) with a computation time of about 40 minutes. We also fit the model using an MCMC run of 8 chains with 10,000 iterations (including a warmup of 2,000) each for a total of 64,000 usable iterations, using the `tmbstan` package (Monnahan and Kristensen, 2018) at a computation time of approximately 66 hours per chain. Figure 2 shows the posterior mean incidence rates $\lambda(\cdot)$ obtained from 100 independent posterior samples from the approximate posterior and from MCMC, as well as mean excess spatial variation $u(\cdot)$ and probability of exceeding 20% risk, $\mathbb{P}[\lambda(\cdot) > 0.2 | \mathbf{Y}]$. Table 2 shows the posterior mean and standard deviation for the regression coefficients and nonlinear parameters computed using the ELGM procedure and MCMC. Finally, Figure 3 shows the posteriors for $(\tau^{-1/2}, \sigma, \rho)$ computed using our approach, the full Laplace approximation, and MCMC. The ELGM approach generally matches the MCMC output closely, and in the case of the posteriors for the nonlinear parameters (Figure 3), appears more accurate than the full Laplace approximation of Nandi et al. (2020).

6.2 Spatial survival regression with partial likelihood

The Cox Proportional Hazards model with partial likelihood is the standard model for survival analysis problems. The partial (log) likelihood has a Hessian matrix which is completely dense and hence is not compatible with the LGM framework, and is in fact the most computationally-intensive type of ELGM. In this example we fit this model with the hazard depending on a latent spatial point process, a very challenging model to fit.

We consider a classic dataset of Leukaemia survival times in northern England where the goal is to infer the spatial variation in survival time. These data have been analyzed using survival models with parametric hazard functions (Henderson et al., 2002; Lindgren

n	Time (seconds)			Scaled L_2 -norm of difference
	ELGM	R-INLA (8 threads)	R-INLA (single threaded)	
1,000	17.1	16.9	27.8	0.0462
10,000	25.5	20.3	31.2	0.0118
100,000	67.2	50.2	74.0	0.00812
1,000,000	715	905	781	0.00624
7,283,575	6,475	28,079	14,755	0.00705

Table 1: Run times and scaled L_2 norm of difference in posterior means of \mathbf{W} for ELGM and R-INLA run on the opioid treatment centre example of §5.

Param.	Mean		SD		2.5%		97.5%	
	ELGM	MCMC	ELGM	MCMC	ELGM	MCMC	ELGM	MCMC
β_0	-3.054	-3.055	0.311	0.379	-3.659	-3.756	-2.441	-2.257
β_{elev}	-0.466	-0.460	0.188	0.184	-0.835	-0.821	-0.096	-0.099
β_{vege}	0.384	0.381	0.203	0.202	-0.015	-0.015	0.780	0.774
β_{1st}	0.202	0.178	0.263	0.259	-0.315	-0.340	0.716	0.679
$\tau^{-1/2}$	0.660	0.657	0.087	0.084	0.502	0.502	0.847	0.832
σ	1.022	1.033	0.198	0.195	0.666	0.693	1.446	1.457
ρ	2.574	2.558	0.984	0.920	1.316	1.355	5.003	4.854

Table 2: Coefficient and nonlinear parameter posterior summaries from the ELGM procedure and MCMC, for the Malaria example of §6.1.

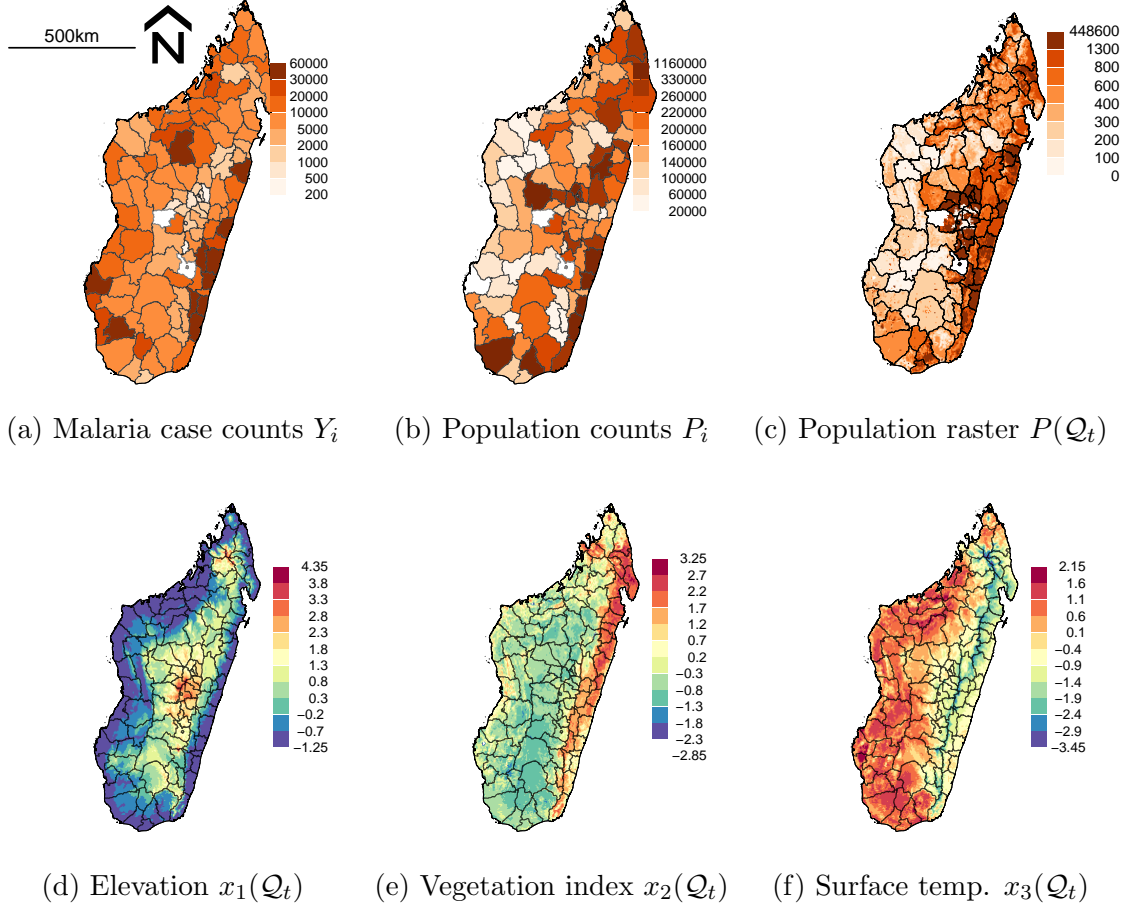
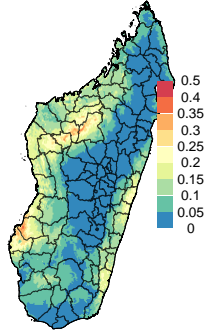
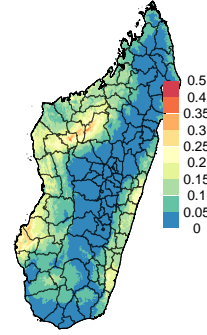


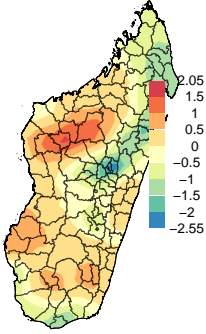
Figure 1: Case counts Y_i , population counts within each polygon $P_i = \int_{S_i} P(\mathbf{s})d\mathbf{s}$ and at the pixel level $P(Q_t)$, and covariate rasters $\mathbf{x}(Q_t) = [1, x_1(Q_t), x_2(Q_t), x_3(Q_t)]$, $t \in [T]$ for Malaria incidence in Madagascar, §6.1.



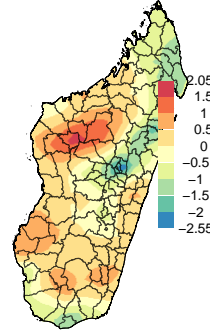
(a) $\mathbb{E}[\lambda(\mathcal{Q}_t)|\mathbf{Y}]$, ELGM



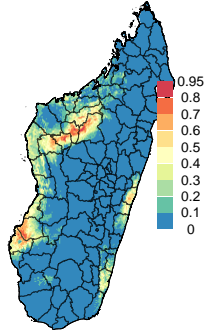
(b) $\mathbb{E}[\lambda(\mathcal{Q}_t)|\mathbf{Y}]$, MCMC



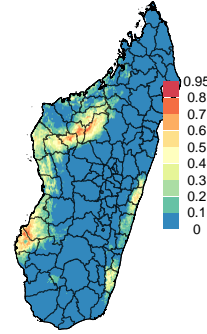
(c) $\mathbb{E}[u(\mathcal{Q}_t)|\mathbf{Y}]$, ELGM



(d) $\mathbb{E}[u(\mathcal{Q}_t)|\mathbf{Y}]$, MCMC



(e) $\mathbb{P}[\lambda(\mathcal{Q}_t) > 0.2|\mathbf{Y}]$, ELGM



(f) $\mathbb{P}[\lambda(\mathcal{Q}_t) > 0.2|\mathbf{Y}]$, MCMC

Figure 2: Posterior summaries from the ELGM procedure and MCMC on the grid $\mathcal{Q}_t, t \in [T]$, for the Malaria example of §6.1.

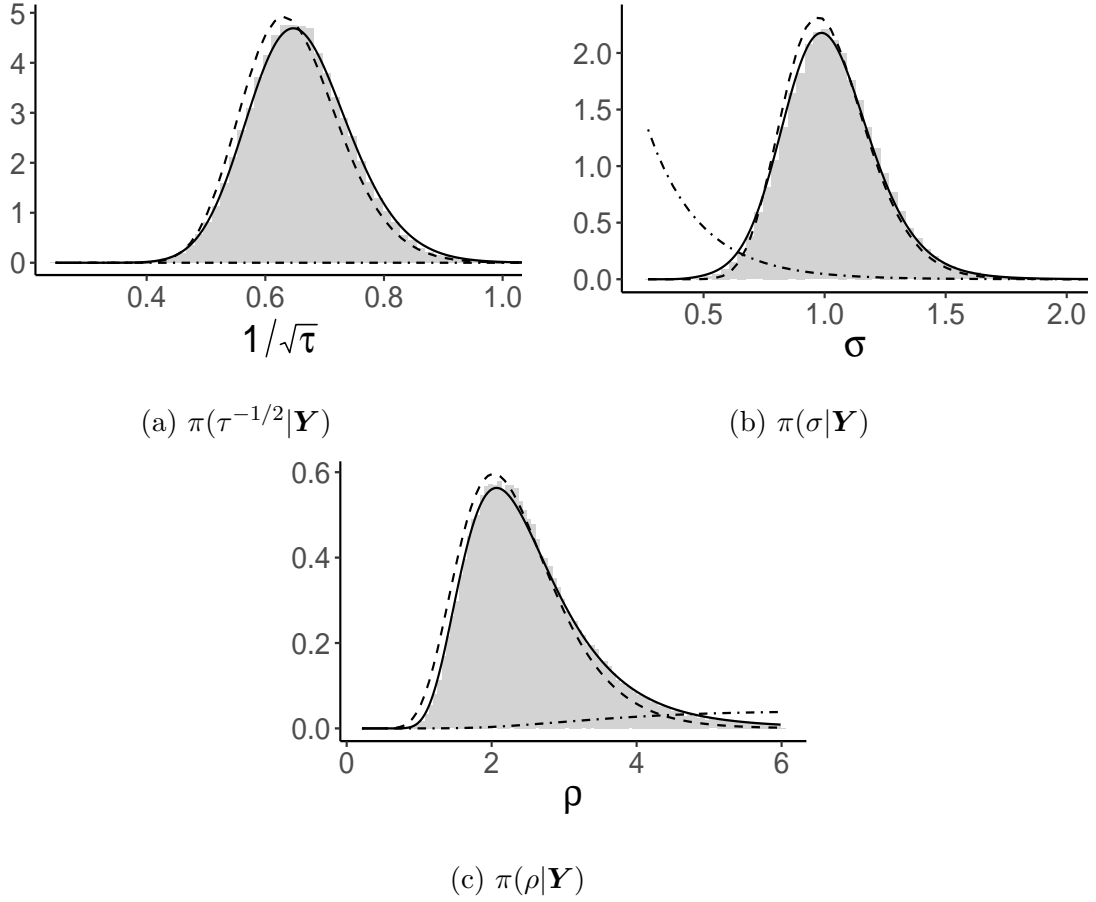


Figure 3: Approximate posteriors for $\tau^{-1/2}, \sigma, \rho$ using the ELGM procedure (—) and the Laplace approximation of Nandi et al. (2020) (- - -), along with posterior samples from MCMC (■) and prior (- · -), for the Malaria example of §6.1.

et al., 2011), resulting in simpler computations than when using partial likelihood. More recently Martino et al. (2011) adapt the methodology of Rue et al. (2009) to analyze these data using a semi-parametric hazard model which is still less computationally intensive than using partial likelihood, and where spatial variation is restricted to occur between predefined geographical regions. Unlike these previous analyses, we fit a Cox Proportional Hazards model using partial likelihood and a continuously-varying spatial model using the exact observed point locations, which is feasible in the ELGM framework introduced in this paper.

The data consist of the survival times of $n = 1043$ Leukaemia patients in northern England. Of these $n_0 = 879$ were observed to die during the study period and $n - n_0 = 164$ were right-censored. Denote the study region by $\mathcal{M} \subset \mathbb{R}^2$. Each subject has a point location of residence $\mathbf{s}_i \in \mathcal{M}$, and covariate vector $\mathbf{x}_i \in \mathbb{R}^p$ with $p = 4$ containing age, sex, white blood cell count (WBC), and the Townsend Deprivation Index (TPI), a measure of social deprivation. Let $Y_i, i \in [n]$ denote the survival time of the i^{th} subject. For convenience suppose $0 < Y_1 < \dots < Y_{n_0}$ are observed and $\{Y_i, i = n_0 + 1, \dots, n\}$ are censored. We use the following hierarchical model:

$$\begin{aligned}\pi(\mathbf{Y}|\boldsymbol{\lambda}) &= \prod_{i=1}^{n_0} \frac{\lambda_i}{\sum_{j=i}^n \lambda_j}, \\ \eta_i &= \log \lambda_i = \beta_0 + \mathbf{x}_i^T \boldsymbol{\beta} + u(\mathbf{s}_i), i \in [n], \\ u(\mathbf{s}) &\sim \mathcal{GP}[0, M_\nu(\cdot; \sigma, \rho)], \\ \text{Cov}[u(\mathbf{s} + \mathbf{h}), u(\mathbf{s})] &= M_\nu(\|\mathbf{h}\|; \sigma, \rho), \mathbf{s} \in \mathcal{M}, \mathbf{h} \in \mathbb{R}^2, \\ \mathcal{J}_i &= \{i, \dots, n\}.\end{aligned}$$

Because $\mathcal{J}_1 = [n]$ we have $k, l \in \mathcal{J}_1$ for every $k, l \in [n]$ and hence $\mathbf{C}_{\boldsymbol{\eta}, \boldsymbol{\theta}_1}$ is a fully dense matrix (§3).

For the spatially-varying Gaussian process $u(\cdot)$ we use a Matern covariance function as in §6.1, however we do not use a piecewise constant approximation to $u(\cdot)$ with the sparse approximation to its precision matrix, and instead evaluate the dense covariance matrix at the observed point locations. This is a reasonable strategy in this example because the Hessian is already dense, so working with a dense prior precision matrix would not be

expected to add much additional complexity. Here, $\mathbf{U} = \{u(\mathbf{s}_i) : i \in [n]\}$ with dimension $d = n$. The model for \mathbf{U} is:

$$\begin{aligned}\mathbf{U}|\boldsymbol{\theta}_2 &\sim \text{Normal}(0, \boldsymbol{\Sigma}), \\ \Sigma_{jk} &= M_\nu(\|\mathbf{s}_j - \mathbf{s}_k\|; \sigma, \rho), j, k \in [n],\end{aligned}$$

where, as in §6.1, $M_\nu(\cdot; \sigma, \rho)$ is a Matern covariance function with fixed shape $\nu = 1$, and standard deviation σ and range ρ in the parametrization of Brown (2015). The nonlinear parameters are $\boldsymbol{\theta} = (\log \sigma, \log \rho)$. Again as in §6.1 we follow Fuglstad et al. (2019) and choose independent Exponential priors on σ and ρ^{-1} which satisfy $\mathbb{P}(\sigma > 1) = \mathbb{P}(\rho < 20\text{km}) = 0.5$.

To jointly infer the values of $\mathbf{U}^* = \{u(\mathbf{s}_l^*) : l \in [L]\}$ for any (new) locations $\{\mathbf{s}_l^* : l \in [L]\} \subset \mathcal{M}$, $L \in \mathbb{N}$ we simulate from the approximate predictive distribution of $\mathbf{U}^*|\mathbf{Y}$. Specifically, with $\mathbf{W} = (\mathbf{U}, \boldsymbol{\beta})$ we draw from $\mathbf{W}|\mathbf{Y}$ according to Algorithm 1 and then from $\mathbf{U}^*|\mathbf{U}$ using methods implemented in the `RandomFields` package (Schlather et al., 2015). This procedure makes explicit use of the full joint posterior approximation $\tilde{\pi}(\mathbf{W}|\mathbf{Y})$.

Table 3 shows the posterior medians and credible regions for the coefficients of age, sex, Cell Count (WBC) and Deprivation (TPI), along with those for the the nonlinear parameters. The use of partial likelihood means that these are obtained without assumptions on the form of the baseline hazard. Figure 4 shows the approximate posterior distributions of the two nonlinear parameters in the Matern covariance function as well as the approximate posterior mean and 20% exceedence probabilities obtained from 100 draws from $\mathbf{U}^*|\mathbf{Y}$ for a fine grid of points $\mathbf{s}_1^*, \dots, \mathbf{s}_L^*$, $L = 58,215$ obtained by laying a 400×200 square over the study area and taking the intersection of this square with the map. The use of exact point locations and simulation on a fine grid leads to a higher-resolution estimate than that of Henderson et al. (2002) and Lindgren et al. (2011).

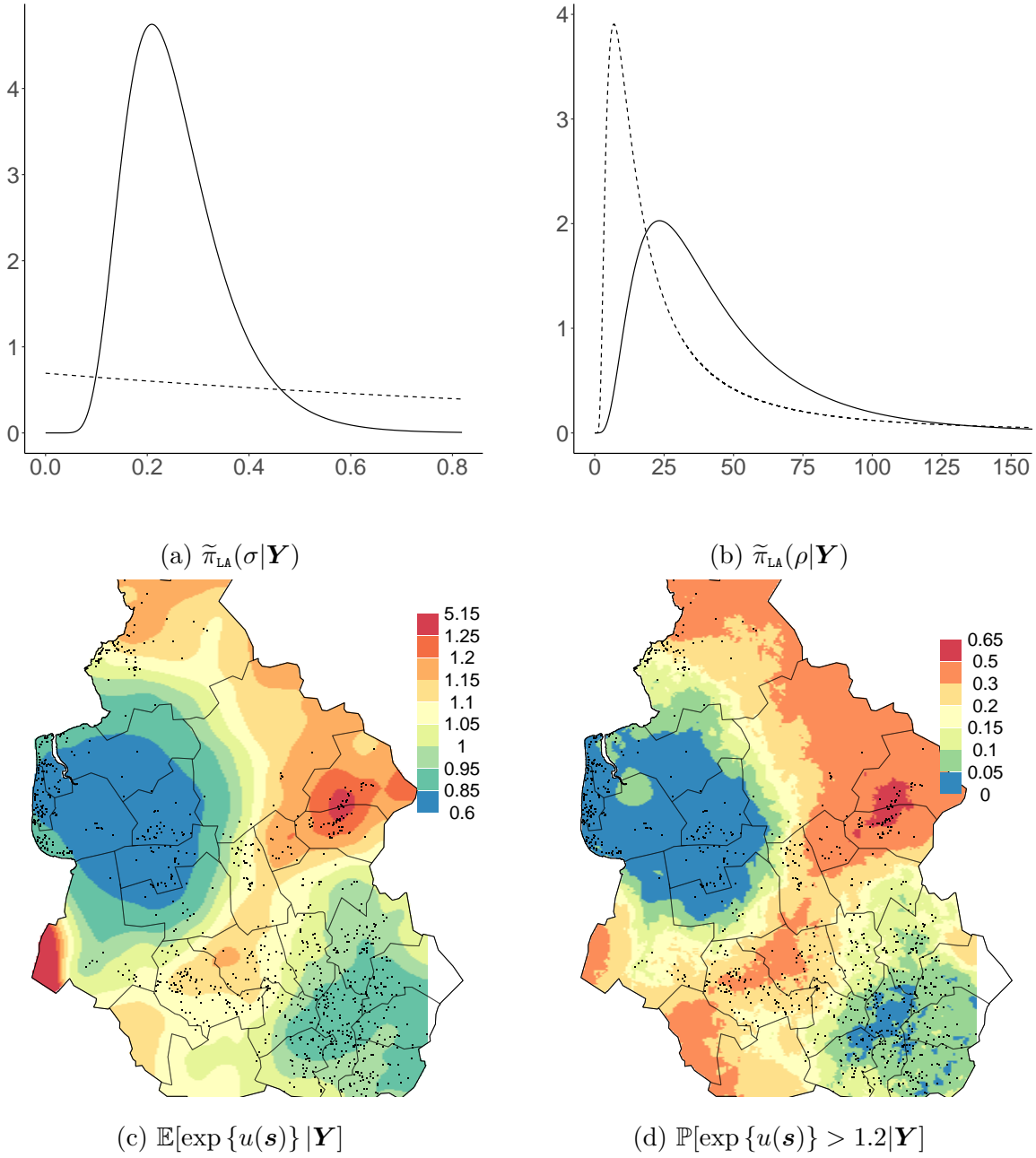


Figure 4: (Top) Priors (---) and approximate posterior distributions (—) for (a) the spatial standard deviation and (b) range (KM, density $\times 10^5$). (Bottom) maps showing (c) point locations of deaths (\cdot) and approximate posterior mean excess spatial variation and (d) approximate posterior probability of exceeding 20% excess spatial variation for the spatial survival analysis of §6.2

Table 3: Posterior moments and quantiles for fixed effects and nonlinear parameters for the Leukaemia data of Example 6.2.

Variable	Mean	SD	2.5%	97.5%
Age	0.029	0.002	0.024	0.033
Male	0.029	0.069	-0.107	0.171
Cell Count	0.003	0.001	0.002	0.004
Deprivation	0.027	0.009	0.009	0.046
SD, σ	0.257	0.095	0.115	0.499
Range, ρ (KM)	44.2	32.0	9.77	134

6.3 Estimating the mass profile of the Milky Way with measurement error

In this section we provide an example of an ELGM that, although we obtain reasonable results, pushes the computational boundaries of the current approach, motivating future work. In a series of papers, Eadie and Harris (2016), Eadie et al. (2017), Eadie et al. (2018) and Eadie and Juric (2019) develop and test a model for estimating the mass of the Milky Way Galaxy using position and velocity measurements of star clusters in its orbit. They use a physical model which implies a probability distribution for the position and velocity of star clusters which depends on parameters that determine the mass of the Galaxy at any radial distance from its centre. This distribution is used in a hierarchical model which incorporates measurement uncertainties for the multivariate response and missing data. Inference is based on posterior distributions for the parameters of interest, upon which estimates and uncertainty quantification for the mass of the Galaxy are based.

Throughout these papers, posteriors are computed using MCMC which requires extensive user tuning (Eadie et al., 2017). Bilodeau et al. (2021) and Stringer (2021) fit the simpler model from Eadie and Harris (2016)—which does not include measurement uncertainties—using AGHQ only, observing significantly improved run times when compared to MCMC and not requiring user tuning. Here we extend their analysis and present

similar results to Eadie et al. (2017) using the ELGM procedure with a running time faster than that reported by Eadie et al. (2017) and no user tuning, although we simplify some aspects of inference for purposes of illustration.

We describe only the relevant statistical details of this example; the physical details are well beyond the scope of this paper. Let $\mathbf{y}_i = (y_{i,1}, y_{i,2}, y_{i,3}, y_{i,4})$ denote the four kinematic measurements taken for the i^{th} star cluster: position, line-of-sight velocity, proper motion in right-ascention corrected for declination, and proper motion in declination, and let $\mathbf{Y} = \{\mathbf{y}_i : i \in [n]\}$. These *heliocentric* measurements are taken with respect to the position and motion of the sun, and are converted to *galactocentric* position and motion relative to the centre of the Galaxy using a deterministic, nonlinear transformation $\Omega : \mathbb{R}^4 \rightarrow \mathbb{R}^4$. The probability distribution relating the measurements to the mass of the Galaxy is defined in this galactocentric frame of reference. Prior to transformation, each heliocentric measurement is subject to a random measurement error ω_i with mean zero and fixed standard deviation Δ_i which is reported as part of the measurement process.

For simplicity we consider only clusters with complete kinematic measurements and include measurement errors on the position and line-of-sight velocity only, defining $\omega_i = (\omega_{i,1}, \omega_{i,2})$, $\mathbf{W} = \{\omega_i : i \in [n]\}$, and letting $\mathbf{y}_i^* = (y_{i,1} + \omega_{i,1}, y_{i,2} + \omega_{i,2}, y_{i,3}, y_{i,4})$ for $i \in [n]$. There are $n = 70$ star clusters with complete data. A probability distribution $\pi[\Omega(\mathbf{y}_i)|\boldsymbol{\theta}]$ over the galactocentric measurements $\Omega(\mathbf{y}_i), i \in [n]$ depends on parameters $\boldsymbol{\theta} = (\Psi_0, \gamma, \alpha, \beta)$, and the mass of the Galaxy at radial distance r kiloparsecs (kpc) from its centre is given as $M_{\boldsymbol{\theta}}(r) = \gamma\Psi_0r^{1-\gamma}$. This is the object of inferential interest. Parameter transformations and strongly-informative priors on $\boldsymbol{\theta}$ are set according to the extensive discussion in Eadie and Harris (2016) and as reported by Bilodeau et al. (2021) and Stringer (2021). For further detail, refer to Eadie and Harris (2016) and Eadie et al. (2017) as well as Bilodeau et al. (2021) and Stringer (2021).

The model is as follows:

$$\begin{aligned} \pi(\mathbf{y}|\mathbf{W}, \boldsymbol{\theta}) &= \prod_{i=1}^n \pi[\Omega(\mathbf{y}_i^*)|\boldsymbol{\theta}], \\ \omega_i &\stackrel{ind}{\sim} \text{Normal}[0, \text{diag}(\Delta_i)], i \in [n], \\ \mathcal{J}_i &= \{\{i, 1\}, \{i, 2\}\}, \end{aligned} \tag{8}$$

where $i \in [n]$. The measurement standard deviations $\Delta_i = (\Delta_{i1}, \Delta_{i2}), i \in [n]$ are reported for each cluster and taken as fixed and known. The strongly-informative priors are $\Psi_0 \sim \text{Unif}(1, 200)$, $\gamma \sim \text{Unif}(0.3, 0.7)$, $\alpha - 3 \sim \text{Gamma}(1, 4.6)$ and $\beta \sim \text{Unif}(-0.5, 1)$ (Eadie and Harris, 2016). The index sets $\mathcal{J}_i, i \in [n]$ have $|\mathcal{J}_i| = 2 > 1$ for each $i \in [n]$ because the observations are multivariate. This is therefore an example of an ELGM compatible with our methodology, but not an LGM.

We fit this model (Algorithm 1), obtaining results that are broadly comparable to those reported by Eadie and Harris (2016) and Eadie et al. (2017) accounting for the priors and data inclusion rules used. Figure 5 shows the posterior distributions for $\Psi_0, \gamma, \alpha, \beta$ and Figure 6 shows the estimated cumulative mass profile $M_{\theta}(r)$ of the Galaxy for chosen values of r . While the posterior mean and standard deviation of $M_{\theta}(r)$ are straightforward to obtain using quadrature, an approximation to the posterior density of a nonlinear, trans-dimensional transformation of θ is in general difficult to obtain using our procedure as no algorithm is available to draw samples from $\tilde{\pi}_{\text{ta}}(\theta|\mathbf{Y})$, so we instead report the posterior mean along with pointwise one and two standard deviation bands for each value of $r = 1, 2, \dots, 150$.

Despite the reasonable results we obtained using the ELGM procedure as described directly in Algorithm 1, there are several computational challenges in this example which we leave to future work. The parameters \mathbf{W} and θ are subject to complicated nonlinear constraints implied by the underlying physics, and these constraints depend both on θ and $\widehat{\mathbf{W}}_{\theta}$. Advanced methods for optimization in the presence of such nonlinear constraints are readily available (see the IPOPT software of Wachter and Biegler (2006) and corresponding `ipoptr` R package) and this is done by Bilodeau et al. (2021) and Stringer (2021) without the measurement errors. However, in the presence of measurement errors this would require the derivatives of the constraints which involves differentiating through $\widehat{\mathbf{W}}_{\theta}$ with respect to θ . This is a challenging task which has recently been investigated in a related context by Margossian et al. (2020), and we leave its implementation here to future work. We also do not incorporate missing data into the hierarchical model as done by Eadie et al. (2017) and Eadie and Juric (2019). Nonetheless, our framework appears to give reasonable

results in very moderate computational time, and is a promising step in the development of approximate Bayesian inference methods for fitting models of this level of complexity.

7 Discussion

We have defined a novel class of Extended Latent Gaussian Models and developed approximate Bayesian inference methodology for this class. The method relies less on sparse matrix algorithms but also depends on matrices of smaller size than previous approaches, and we have shown one example of a simple model in which our procedure appears to run faster for large datasets. We have discussed the convergence properties of the approximations including how each approximation contributes to the overall error, identified limitations of existing convergence results for approximations in this context, and described how this may be used in the development of future convergence theory pertaining to approximate Bayesian inference. We demonstrated three challenging examples of ELGMs and fit them with our procedure: inference for a continuous spatial field using aggregated point process data, including a comparison to MCMC; a Cox Proportional hazards model with partial likelihood for mapping the spatial variation in Leukaemia survival times; and an astrophysical model for estimating the mass of the Milky Way galaxy accounting for multivariate measurement uncertainties. The core method (Algorithm 1) is implemented in the open source `aghq` package in the R language.

There are a number of compelling avenues for future research. While we have discussed the asymptotic error of $\tilde{\pi}(\mathbf{W}|\mathbf{Y})$ (§4), several authors (Rue and Martino, 2007; Rue et al., 2009) have pointed out that the use of Gaussian approximations $\tilde{\pi}_g(\mathbf{W}|\mathbf{Y}, \boldsymbol{\theta})$ may be inaccurate in finite samples. Rue et al. (2009) and Wood (2020) introduce approximations which are demonstrably more accurate than the Gaussian, however work for *marginal* posterior distributions only. In contrast, our procedure depends on access to fast independent sampling from the *joint* posterior (Algorithm 1), which we use to compute any complicated posterior summary in a straightforward manner (§6.1, §6.2). As noted in the discussion to Rue et al. (2009) and by us in §3, this is a compelling practical advantage of MCMC algorithms, and we believe it is important to retain this advantage when developing methods for approxi-

mate Bayesian inference. In future work we plan to develop a more accurate multivariate skew-Normal approximation to this distribution that still admits fast independent samples.

Establishing convergence of the error incurred when applying the AGHQ rule based on $\tilde{\pi}_{\text{LA}}(\boldsymbol{\theta}|\mathbf{Y})$ a second time when integrating $\pi(\mathbf{W}, \boldsymbol{\theta}|\mathbf{Y})$ is required to further study the asymptotic properties of the approximation error even in the simple case of a fixed-dimensional asymptotic regime, and this will be a subject of future work. Further, as we point out (§4), additional work may be needed to establish convergence of $\tilde{\pi}(\mathbf{W}|\mathbf{Y})$ on a problem-specific basis. Accommodating mis-specified models seems feasible given recent work in the area of asymptotic normality of posterior distributions under misspecification (Kleijn and van der Vaart, 2012) which we already invoke in proving Lemma 1 in Appendix A, but may have to be approached on a model-specific basis, in combination with results on convergence of approximations to the continuous processes $u(\cdot)$ (e.g. Lindgren et al. 2011; Simpson et al. 2016). The high-dimensional asymptotic regime is less clear. Shun and McCullagh (1995) discuss the difficulty of applying Laplace approximations when $\dim(\mathbf{W}) = O(n)$; more recently, Baghishania and Mohammadzadeh (2012) do show asymptotic normality of a posterior distribution in a high-dimensional regime under certain specific assumptions. Characterizing for which high-dimensional ELGMs convergence holds is an interesting future direction. These considerations fall within what is becoming an active area of research in the theory pertaining to approximate Bayesian inference as discussed by Bilodeau et al. (2021).

The purpose of developing a novel statistical method is ultimately adoption by a wider audience of both statisticians and other scientists, and development of open-source software will play an integral part in this as it has for the methods of Rue et al. (2009). The `aghq` package implements Algorithm 1, automating the majority of our method for ELGMs. The user still has to input the unnormalized log-posterior $\pi(\mathbf{W}, \boldsymbol{\theta}, \mathbf{Y})$, and therefore this package is more suitable for statisticians who wish to fit new ELGMs as opposed to general scientists who wish to fit existing ELGMs to their data. We plan to implement an *ecosystem* of individual R packages which make specific ELGMs such as those in §5 and §6 available to a general scientific audience. This strategy will enable both statisticians and general

scientists to use the ELGM inference methodology in their research.

Acknowledgements

The authors are grateful for helpful comments provided by Blair Bilodeau and Yanbo Tang.

A Asymptotic Convergence of Posterior Approximations

In this section we investigate the approximation error in more detail. In §A.2 we split the error into three terms which isolate the effects of the three types of approximations (Gaussian, Laplace, quadrature). We state (§A.2) and prove (§A.3) Lemmas 1 and 2 which establish the convergence of the error from the first two sources. As discussed in §4, owing to limitations with the theory pertaining to AGHQ in the present context we provide only a heuristic argument for convergence of the quadrature error, leaving its rigorous establishment to future work.

A.1 Preliminaries

We begin with some preliminaries. We repeat definition of the following quantities (Algorithm 1):

$$\pi(\mathbf{W}, \boldsymbol{\theta}, \mathbf{Y}) = \pi(\mathbf{Y}|\mathbf{W}, \boldsymbol{\theta})\pi(\mathbf{W}|\boldsymbol{\theta})\pi(\boldsymbol{\theta}),$$

$$\widehat{\mathbf{W}}_{\boldsymbol{\theta}} = \operatorname{argmax}_{\mathbf{W}} \pi(\mathbf{W}, \mathbf{Y}, \boldsymbol{\theta}), \quad \mathbf{H}_{\boldsymbol{\theta}}(\mathbf{W}) = -\partial_{\mathbf{W}}^2 \log \pi(\mathbf{W}, \mathbf{Y}, \boldsymbol{\theta}),$$

$$\tilde{\pi}_{\text{LA}}(\boldsymbol{\theta}, \mathbf{Y}) \propto \left| \mathbf{H}_{\boldsymbol{\theta}}(\widehat{\mathbf{W}}_{\boldsymbol{\theta}}) \right|^{-1/2} \pi(\widehat{\mathbf{W}}_{\boldsymbol{\theta}}, \boldsymbol{\theta}, \mathbf{Y}),$$

$$\widehat{\boldsymbol{\theta}} = \operatorname{argmax}_{\boldsymbol{\theta}} \tilde{\pi}_{\text{LA}}(\boldsymbol{\theta}, \mathbf{Y}), \quad \mathbf{H}(\boldsymbol{\theta}) = -\partial_{\boldsymbol{\theta}}^2 \log \tilde{\pi}_{\text{LA}}(\boldsymbol{\theta}, \mathbf{Y}), \quad \mathbf{H}(\boldsymbol{\theta})^{-1} = \mathbf{L}\mathbf{L}^T \text{ (Cholesky)},$$

$K = K_1^s$: number of quadrature points; $\{\mathbf{x}_k, \omega_k^*\}_{k=1}^K$: points and weights from a standard K_1 -point GHQ quadrature rule in s dimensions (Bilodeau et al., 2021, §2.3),

$\boldsymbol{\theta}^k = \mathbf{L}\mathbf{x}_k + \widehat{\boldsymbol{\theta}}$, $\omega_k = |\mathbf{L}| \omega_k^*$, $k \in [K]$: AGHQ points and weights (Bilodeau et al., 2021, §2.4).

Also,

$$\pi(\mathbf{W}|\mathbf{Y}, \boldsymbol{\theta}) \propto \pi(\mathbf{Y}|\mathbf{W}, \boldsymbol{\theta})\pi(\mathbf{W}|\boldsymbol{\theta}),$$

$$\tilde{\pi}_g(\mathbf{W}|\mathbf{Y}, \boldsymbol{\theta}) = (2\pi)^{-m/2} \left| \mathbf{H}_{\boldsymbol{\theta}}(\widehat{\mathbf{W}}_{\boldsymbol{\theta}}) \right|^{1/2} \exp \left[-\frac{1}{2} (\mathbf{W} - \widehat{\mathbf{W}})^T \mathbf{H}_{\boldsymbol{\theta}}(\widehat{\mathbf{W}}_{\boldsymbol{\theta}}) (\mathbf{W} - \widehat{\mathbf{W}}) \right].$$

Throughout we assume that

$$M = \sup_{\boldsymbol{\theta} \in \mathbb{R}^s} \pi(\boldsymbol{\theta}|\mathbf{Y}) < \infty$$

with \mathbb{P}_0 -probability 1, which is an implicit assumption in using the mode $\widehat{\boldsymbol{\theta}}$ for inference anyways. We further assume the necessary conditions on the model such that $\pi(\mathbf{W}|\mathbf{Y}, \boldsymbol{\theta}^k)$ satisfies Local Asymptotic Normality for all $k \in [K]$, $K \in \mathbb{N}$; see Kleijn and van der Vaart (2012, §2.1).

A.2 Approximation Error

By the triangle inequality:

$$\begin{aligned} & \sup_{\mathcal{K} \in \mathcal{B}(\mathbb{R}^m)} \left| \int_{\mathcal{K}} \pi(\mathbf{W}|\mathbf{Y}) - \tilde{\pi}(\mathbf{W}|\mathbf{Y}) d\mathbf{W} \right| \\ & \leq \sup_{\mathcal{K} \in \mathcal{B}(\mathbb{R}^m)} \left| \int_{\mathcal{K}} \sum_{k=1}^K [\tilde{\pi}_g(\mathbf{W}|\mathbf{Y}, \boldsymbol{\theta}^k) - \pi(\mathbf{W}|\mathbf{Y}, \boldsymbol{\theta}^k)] \tilde{\pi}_{\text{LA}}(\boldsymbol{\theta}^k|\mathbf{Y}) \omega_k d\mathbf{W} \right| \\ & \quad + \sup_{\mathcal{K} \in \mathcal{B}(\mathbb{R}^m)} \left| \int_{\mathcal{K}} \sum_{k=1}^K \pi(\mathbf{W}|\mathbf{Y}, \boldsymbol{\theta}^k) \pi(\boldsymbol{\theta}^k|\mathbf{Y}) \left[\frac{\tilde{\pi}_{\text{LA}}(\boldsymbol{\theta}^k|\mathbf{Y})}{\pi(\boldsymbol{\theta}^k|\mathbf{Y})} - 1 \right] \omega_k d\mathbf{W} \right| \\ & \quad + \sup_{\mathcal{K} \in \mathcal{B}(\mathbb{R}^m)} \left| \int_{\mathcal{K}} \pi(\mathbf{W}|\mathbf{Y}) - \sum_{k=1}^K \pi(\mathbf{W}, \boldsymbol{\theta}^k|\mathbf{Y}) \omega_k d\mathbf{W} \right|. \end{aligned}$$

We state the following two Lemmas pertaining to the convergence of the first two terms :

Lemma 1.

$$\sup_{\mathcal{K} \in \mathcal{B}(\mathbb{R}^m)} \left| \int_{\mathcal{K}} \sum_{k=1}^K [\tilde{\pi}_g(\mathbf{W}|\mathbf{Y}, \boldsymbol{\theta}^k) - \pi(\mathbf{W}|\mathbf{Y}, \boldsymbol{\theta}^k)] \tilde{\pi}_{\text{LA}}(\boldsymbol{\theta}^k|\mathbf{Y}) \omega_k d\mathbf{W} \right| \xrightarrow{\mathbb{P}_0} 0.$$

Lemma 2.

$$\sup_{\mathcal{K} \in \mathcal{B}(\mathbb{R}^m)} \left| \int_{\mathcal{K}} \sum_{k=1}^K \pi(\mathbf{W}|\mathbf{Y}, \boldsymbol{\theta}^k) \pi(\boldsymbol{\theta}^k|\mathbf{Y}) \left[\frac{\tilde{\pi}_{\text{LA}}(\boldsymbol{\theta}^k|\mathbf{Y})}{\pi(\boldsymbol{\theta}^k|\mathbf{Y})} - 1 \right] \omega_k d\mathbf{W} \right| \xrightarrow{\mathbb{P}_Q} 0.$$

We defer proof of these Lemmas to Appendix A.3. The third term:

$$\sup_{\mathcal{K} \in \mathcal{B}(\mathbb{R}^m)} \left| \int_{\mathcal{K}} \pi(\mathbf{W}|\mathbf{Y}) - \sum_{k=1}^K \pi(\mathbf{W}, \boldsymbol{\theta}^k|\mathbf{Y}) \omega_k d\mathbf{W}, \right|$$

is challenging. It represents a nonstandard application of adaptive quadrature. Specifically, the convergence properties of the AGHQ rule depend on it being centered and scaled correctly. However, the mode $\hat{\boldsymbol{\theta}}$ and curvature $\mathbf{H}(\boldsymbol{\theta})$ used to construct this rule are that of $\log \tilde{\pi}_{\text{LA}}(\boldsymbol{\theta}|\mathbf{Y})$, not $\log \pi(\mathbf{W}, \boldsymbol{\theta}|\mathbf{Y})$, and this invalidates convergence results for it. Note that this problem would presumably occur for any adaptive quadrature rule applied in such a nonstandard manner, including the two used by Rue et al. (2009).

To see heuristically that this term converges, define the three modes:

$$\hat{\boldsymbol{\theta}}_1 = \operatorname{argmax}_{\boldsymbol{\theta}} \tilde{\pi}_{\text{LA}}(\boldsymbol{\theta}|\mathbf{Y}), \quad \hat{\boldsymbol{\theta}}_2 = \operatorname{argmax}_{\boldsymbol{\theta}} \pi(\boldsymbol{\theta}|\mathbf{Y}), \quad (\widehat{\mathbf{W}}, \hat{\boldsymbol{\theta}}_3) = \operatorname{argmax}_{\mathbf{W}, \boldsymbol{\theta}} \pi(\mathbf{W}, \boldsymbol{\theta}|\mathbf{Y}).$$

Tierney and Kadane (1986) argue that $\|\hat{\boldsymbol{\theta}}_1 - \hat{\boldsymbol{\theta}}_2\| \xrightarrow{\mathbb{P}_Q} 0$, and Pace and Salvani (1997, §4.6) argue (§4.6) that $\|\hat{\boldsymbol{\theta}}_2 - \hat{\boldsymbol{\theta}}_3\| \xrightarrow{\mathbb{P}_Q} 0$ as well, although their results pertain to the maximum likelihood estimators rather than posterior modes. Similar results exist for the corresponding Hessians/information matrices. Hence as $n \rightarrow \infty$, expansions based upon the mode and curvature such as those required to prove convergence of AGHQ can be expected to be asymptotically equivalent.

A.3 Proof of Lemmas 1 and 2

Lemma 1. : The Gaussian approximation $\tilde{\pi}_g(\mathbf{W}|\mathbf{Y}, \boldsymbol{\theta}^k)$ is taken around the point $\widehat{\mathbf{W}}_{\boldsymbol{\theta}^k}$, and hence convergence is not immediately implied as it would be by standard asymptotic theory if the mode and curvature of the correct log-posterior $\log \pi(\mathbf{W}, \boldsymbol{\theta}|\mathbf{Y})$ were used for the expansion. This is complicated by the fact that $\tilde{\pi}_g(\mathbf{W}|\mathbf{Y}, \boldsymbol{\theta}^k)$ is a density for \mathbf{W} conditional on \mathbf{Y} in a very complicated manner through the quadrature points $\boldsymbol{\theta}_k$, and hence the sequence of measures corresponding to these densities varies with n . Convergence

in such a complicated setting requires invoking a recent very general result on Bayesian asymptotics in the misspecified setting: we apply Theorem 2.1 from Kleijn and van der Vaart (2012) in order to conclude that for each $k \in [K]$:

$$\sup_{\mathcal{K} \in \mathcal{B}(\mathbb{R}^m)} \left| \int_{\mathcal{K}} \tilde{\pi}_g(\mathbf{W}|\mathbf{Y}, \boldsymbol{\theta}^k) - \pi(\mathbf{W}|\mathbf{Y}, \boldsymbol{\theta}^k) d\mathbf{W} \right| \xrightarrow{\mathbb{P}_0} 0.$$

Now, by the triangle inequality:

$$\begin{aligned} & \sup_{\mathcal{K} \in \mathcal{B}(\mathbb{R}^m)} \left| \int_{\mathcal{K}} \sum_{k=1}^K [\tilde{\pi}_g(\mathbf{W}|\mathbf{Y}, \boldsymbol{\theta}^k) - \pi(\mathbf{W}|\mathbf{Y}, \boldsymbol{\theta}^k)] \tilde{\pi}_{\text{LA}}(\boldsymbol{\theta}^k|\mathbf{Y}) \omega_k d\mathbf{W} \right| \\ & \leq \sum_{k=1}^K \left[\sup_{\mathcal{K} \in \mathcal{B}(\mathbb{R}^m)} \left| \int_{\mathcal{K}} \tilde{\pi}_g(\mathbf{W}|\mathbf{Y}, \boldsymbol{\theta}^k) - \pi(\mathbf{W}|\mathbf{Y}, \boldsymbol{\theta}^k) d\mathbf{W} \right| \right] \tilde{\pi}_{\text{LA}}(\boldsymbol{\theta}^k|\mathbf{Y}) \omega_k. \end{aligned}$$

The result then follows by noting that $\sum_{k=1}^K \tilde{\pi}_{\text{LA}}(\boldsymbol{\theta}^k|\mathbf{Y}) \omega_k = 1$ with \mathbb{P}_0 -probability 1 by definition. \square

Lemma 2. : Tierney and Kadane (1986) show that:

$$\sup_{\boldsymbol{\theta} \in \mathbb{R}^s} \left| \frac{\tilde{\pi}_{\text{LA}}(\boldsymbol{\theta}|\mathbf{Y})}{\pi(\boldsymbol{\theta}|\mathbf{Y})} - 1 \right| \xrightarrow{\mathbb{P}_0} 0,$$

(see also Kass et al. (1990)). Again by the triangle inequality:

$$\begin{aligned} & \sup_{\mathcal{K} \in \mathcal{B}(\mathbb{R}^m)} \left| \int_{\mathcal{K}} \sum_{k=1}^K \pi(\mathbf{W}|\mathbf{Y}, \boldsymbol{\theta}^k) \pi(\boldsymbol{\theta}^k|\mathbf{Y}) \left[\frac{\tilde{\pi}_{\text{LA}}(\boldsymbol{\theta}^k|\mathbf{Y})}{\pi(\boldsymbol{\theta}^k|\mathbf{Y})} - 1 \right] \omega_k d\mathbf{W} \right| \\ & \leq \sum_{k=1}^K \sup_{\mathcal{K} \in \mathcal{B}(\mathbb{R}^m)} \left| \int_{\mathcal{K}} \pi(\mathbf{W}|\mathbf{Y}, \boldsymbol{\theta}^k) d\mathbf{W} \right| \times \pi(\boldsymbol{\theta}^k|\mathbf{Y}) \left| \frac{\tilde{\pi}_{\text{LA}}(\boldsymbol{\theta}^k|\mathbf{Y})}{\pi(\boldsymbol{\theta}^k|\mathbf{Y})} - 1 \right| \omega_k \\ & = \sum_{k=1}^K \pi(\boldsymbol{\theta}^k|\mathbf{Y}) \left| \frac{\tilde{\pi}_{\text{LA}}(\boldsymbol{\theta}^k|\mathbf{Y})}{\pi(\boldsymbol{\theta}^k|\mathbf{Y})} - 1 \right| \omega_k, \end{aligned}$$

using $\sup_{\mathcal{K} \in \mathcal{B}(\mathbb{R}^m)} \left| \int_{\mathcal{K}} \pi(\mathbf{W}|\mathbf{Y}, \boldsymbol{\theta}^k) d\mathbf{W} \right| = 1$ with \mathbb{P}_0 -probability 1 for each $k \in [K]$. Fix $\epsilon, \delta > 0$ and take $N \in \mathbb{N}$ large enough such that for any $n > N$,

$$\mathbb{P} \left(\sup_{\boldsymbol{\theta} \in \mathbb{R}^s} \left| \frac{\tilde{\pi}_{\text{LA}}(\boldsymbol{\theta}|\mathbf{Y})}{\pi(\boldsymbol{\theta}|\mathbf{Y})} - 1 \right| < \epsilon \right) > 1 - \delta.$$

Conditional on the event that $\sup_{\boldsymbol{\theta} \in \mathbb{R}^s} \left| \frac{\tilde{\pi}_{\text{LA}}(\boldsymbol{\theta}|\mathbf{Y})}{\pi(\boldsymbol{\theta}|\mathbf{Y})} - 1 \right| < \epsilon$ we then have:

$$\sum_{k=1}^K \pi(\boldsymbol{\theta}^k|\mathbf{Y}) \left| \frac{\tilde{\pi}_{\text{LA}}(\boldsymbol{\theta}^k|\mathbf{Y})}{\pi(\boldsymbol{\theta}^k|\mathbf{Y})} - 1 \right| \omega_k \leq M\epsilon \sum_{k=1}^K \omega_k.$$

The quadrature weights are $\omega_k = |\mathbf{L}| \omega_k^*$. Appendix C, Lemma 6, Part ii. of Bilodeau et al. (2021) implies that $|\mathbf{L}| \xrightarrow{\mathbb{P}_0} 0$, and for any $K \in \mathbb{N}$ we have $\max_{k=1}^K \omega_k^* < \infty$, from which we conclude that $\sum_{k=1}^K \omega_k \xrightarrow{\mathbb{P}_0} 0$. Since ϵ, δ were arbitrary, the result follows. \square

Remark 1. Tierney and Kadane (1986) further show that the convergence of the marginal Laplace approximation occurs at a faster than usual $O_{\mathbb{P}_0}(n^{-3/2})$ rate for $\boldsymbol{\theta}$ in a $n^{1/2}$ -neighbourhood of $\boldsymbol{\theta}_0$. Bilodeau et al. (2021) show that the AGHQ quadrature points $\{\boldsymbol{\theta}_k\}_{k=1}^K$ satisfy this property, and hence this faster rate of convergence can be expected to hold when AGHQ is used at the quadrature method in this context. It is not clear whether other quadrature rules satisfy this property.

References

- Baghishania, H. and M. Mohammadzadeh (2012). Asymptotic normality of posterior distributions for generalized linear mixed models. *Journal of Multivariate Analysis* 111, 66–77.
- Bates, D. and M. Maechler (2019). *Matrix: sparse and dense matrix classes and methods*. R package version 1.2-18.
- Bilodeau, B., A. Stringer, and Y. Tang (2021). Stochastic convergence rates and applications of adaptive quadrature in Bayesian inference.
- Braun, M. (2014). trustOptim: An R Package for trust region optimization with sparse Hessians. *Journal of Statistical Software* 60(4), 1–16.
- Brown, P. (2015). Model-based Geostatistics the easy way. *Journal of Statistical Software* 63(12).
- Brown, P. and J. Stafford (2021). A root Gaussian Cox process for spatially-aggregated disease incidence data. *In preparation*.
- Diggle, P., P. Moraga, B. Rowlingson, and B. Taylor (2013). Spatial and spatio-temporal

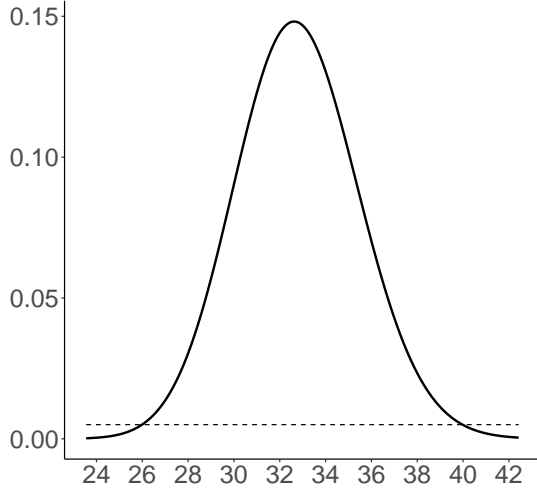
- log-Gaussian Cox processes: extending the geostatistical paradigm. *Statistical Science* 28(4), 542–563.
- Eadie, G. M. and W. E. Harris (2016). Bayesian mass estimates of the Milky Way: the dark and light sides of parameter assumptions. *The Astrophysical Journal* 829(108).
- Eadie, G. M. and M. Juric (2019). The cumulative mass profile of the milky way as determined by globular cluster kinematics from Gaia DR2. *The Astrophysical Journal* 875(159).
- Eadie, G. M., B. Keller, and W. E. Harris (2018). Estimating the Milky Way’s mass via hierarchical Bayes: a blind test on MUGS2 simulated galaxies. *The Astrophysical Journal* 865(72).
- Eadie, G. M., A. Springford, and W. E. Harris (2017). Bayesian mass estimates of the Milky Way: including measurement uncertainties with hierarchical Bayes. *The Astrophysical Journal* 835(167).
- Fuglstad, G.-A., D. Simpson, F. Lindgren, and H. Rue (2019). Constructing priors that penalize the complexity of Gaussian random fields. *Journal of the American Statistical Association* 114(525), 445–452.
- Geyer, C. J. (2020). *trust: Trust Region Optimization*. R package version 0.1-8.
- Henderson, R., S. Shimakura, and D. Gorst (2002). Modelling spatial variation in Leukaemia survival. *Journal of the American Statistical Association* 97(460), 965–972.
- Kass, R. E., L. Tierney, and J. B. Kadane (1990). The validity of posterior expansions based on Laplace’s method. *Bayesian and Likelihood Methods in Statistics and Econometrics*, 473–488.
- Kleijn, B. and A. van der Vaart (2012). The Bernstein von-Mises theorem under misspecification. *Electronic Journal of Statistics* 6, 354–381.
- Kristensen, K., A. Nielson, C. W. Berg, H. Skaug, and B. M. Bell (2016). TMB: automatic differentiation and Laplace approximation. *Journal of statistical software* 70(5).

- Lee, J. S., P. Nguyen, P. E. Brown, J. Stafford, and N. Saint-Jacques (2017). A local-EM algorithm for spatio-temporal disease mapping with aggregated data. *Spatial Statistics* 21, 75–95.
- Li, Y., P. Brown, D. C. Gesink, and H. Rue (2012). Log Gaussian Cox processes and spatially aggregated disease incidence data. *Statistical Methods in Medical Research* 21(5), 479 – 507.
- Lindgren, F. and H. Rue (2015). Bayesian spatial modelling with R-INLA. *Journal of Statistical Software* 63(19), 1–25.
- Lindgren, F., H. Rue, and J. Lindstroom (2011). An explicit link between Gaussian fields and Gaussian Markov random fields: the stochastic partial differential equation approach. *Journal of the Royal Statistical Society, Series B (Statistical Methodology)* 73(4), 423–498.
- Margossian, C. C., A. Vehtari, D. Simpson, and R. Agrawal (2020). Hamiltonian Monte Carlo using an adjoint-differentiated Laplace approximation. *arXiv:2004.12550v3 [stat.CO]*.
- Martino, S., R. Akerkar, and H. Rue (2011). Approximate bayesian inference for survival models. *Scandinavian Journal of Statistics* 38(3), 514 – 528.
- Monnahan, C. and K. Kristensen (2018). No-U-turn sampling for fast Bayesian inference in ADMB and TMB: introducing the adnuts and tmbstan R packages. *PloS one* 13(5).
- Nandi, A. K., T. C. D. Lucas, R. Arambepola, P. Gething, and D. Weiss (2020). disaggregation: an R package for Bayesian spatial disaggregation modelling. *arxiv*.
- Naylor, J. and A. F. M. Smith (1982). Applications of a method for the efficient computation of posterior distributions. *Journal of the Royal Statistical Society, Series C (Applied Statistics)* 31(3), 214–225.
- Pace, L. and A. Salvani (1997). *Principles of statistical inference from a neo-Fisherian perspective*.

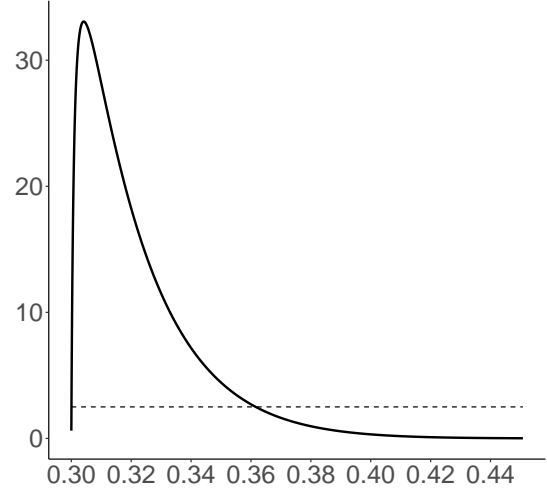
- Rue, H. (2001). Fast sampling of Gaussian Markov random fields. *Journal of the Royal Statistical Society, Series B: Statistical Methodology* 63(2), 325–338.
- Rue, H. and S. Martino (2007). Approximate Bayesian inference for hierarchical Gaussian Markov random field models. *Journal of Statistical Planning and Inference* 137, 3177 – 3192.
- Rue, H., S. Martino, and N. Chopin (2009). Approximate Bayesian inference for latent Gaussian models by using integrated nested Laplace approximations. *Journal of the Royal Statistical Society. Series B (Statistical Methodology)* 71(2), 319 – 392.
- Schlather, M., A. Malinowski, P. J. Menck, M. Oesting, and K. Strokorb (2015). Analysis, simulation and prediction of multivariate random fields with package RandomFields. *Journal of Statistical Software* 63(8).
- Shun, Z. and P. McCullagh (1995). Laplace approximation of high dimensional integrals. *Journal of the Royal Statistical Society, Series B: Statistical Methodology* 57(4), 749–760.
- Simpson, D., J. B. Illian, F. Lindgren, S. H. Sørbye, and H. Rue (2016). Going off grid: computatioanlly efficient inference for log-Gaussian Cox processes. *Biometrika* 103(1), 49–70.
- Simpson, D., H. Rue, T. G. Martins, A. Riebler, and S. H. Sørbye (2017). Penalising model component complexity: A principled, practical approach to constructing priors. *Statistical Science* 32(1).
- Stringer, A. (2021). Implementing adaptive quadrature for Bayesian inference: the aghq package. arXiv:2101.04468.
- Stringer, A., P. Brown, and J. Stafford (2020). Approximate Bayesian inference for case crossover models. *To appear in Biometrics*.
- Tierney, L. and J. B. Kadane (1986). Accurate approximations to posterior moments and marginal densities. *Journal of the American Statistical Association* 81(393).

Wachter, A. and L. T. Biegler (2006). On the implementation of a primal-dual interior point filter line search algorithm for large-scale nonlinear programming. *Mathematical Programming* 106(1), 25 – 57.

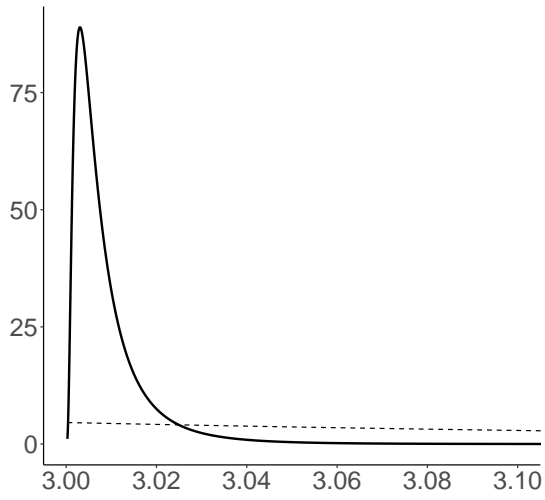
Wood, S. (2020). Simplified integrated nested Laplace approximation. *Biometrika* 107(1), 223–230.



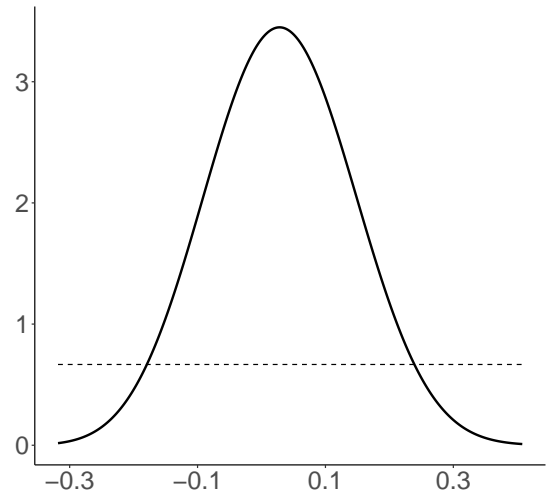
(a) $\tilde{\pi}_{\text{LA}}(\Psi_0|\mathbf{Y})$



(b) $\tilde{\pi}_{\text{LA}}(\gamma|\mathbf{Y})$



(c) $\tilde{\pi}_{\text{LA}}(\alpha|\mathbf{Y})$



(d) $\tilde{\pi}_{\text{LA}}(\beta|\mathbf{Y})$

Figure 5: (a) – (d) prior (– – –) and approximate posterior (—) distributions for the four parameters for the astronomy data of Example 6.3.

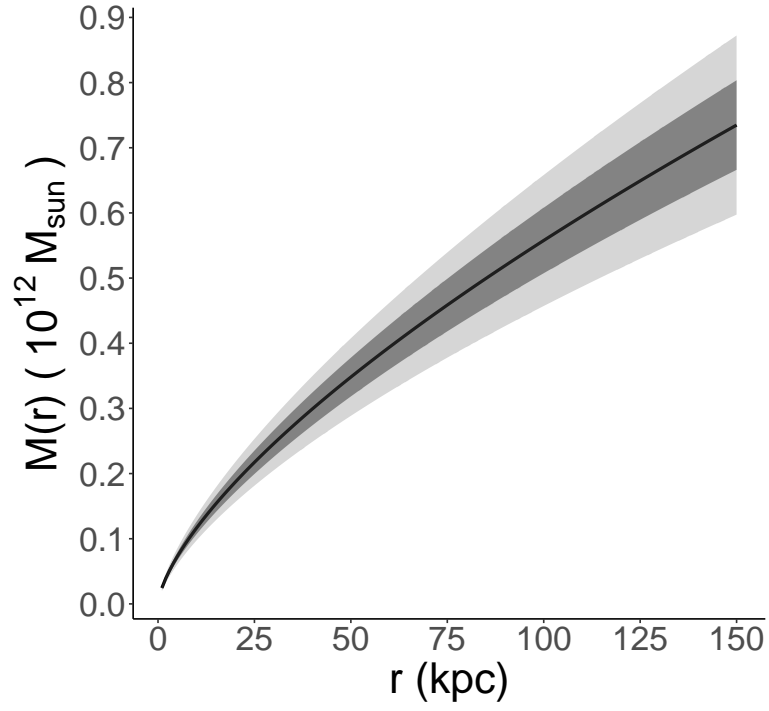


Figure 6: Posterior mean mass of the Milky Way Galaxy relative to the mass of the sun as a function of radial distance from Galaxy centre in kiloparsecs (kpc) ($M_{\theta}(r)$, —), with one- (dark) and two- (light) standard deviation bands for the astronomy data of Example 6.3.